Geomorphology 408 (2022) 108251

Contents lists available at ScienceDirect

Geomorphology

journal homepage: www.journals.elsevier.com/geomorphology

Age, origin and palaeoclimatic implications of peri- and paraglacial boulder-dominated landforms in Rondane, South Norway

Philipp Marr [a,d,*], Stefan Winkler [b], Svein Olaf Dahl [c], Jörg Löffler [d]

[a] University of Vienna, Department of Geography and Regional Research, Geomorphological Systems and Risk Research, Universitätsstraße 7, 1010 Wien, Austria
[b] University of Würzburg, Department of Geography and Geology, Am Hubland, 97074 Würzburg, Germany
[c] Department of Geography, University of Bergen, Fosswinckelsgate 6, 5020 Bergen, Norway
[d] University of Bonn, Department of Geography, Meckenheimer Allee 166, 53115 Bonn, Germany

ARTICLE INFO

Keywords:
Periglacial landforms
Holocene
Climate variability
Schmidt-hammer exposure-age dating (SHD)

ABSTRACT

Boulder-dominated landforms of periglacial, paraglacial and related origin constitute a valuable, but often unexplored source of palaeoclimatic and morphodynamic information. The timing of landform development initiation and its subsequent stabilization can be linked to past climatic conditions offering the potential to reconstruct cold climatic periods. In this study, Schmidt-hammer exposure-age dating (SHD) was applied to a variety of boulder-dominated landforms (sorted stripes, blockfield, rock-slope failure, paraglacial alluvial fan) in Rondane, eastern South Norway for the first time. On the basis of old and young control points a regional SHD calibration curve was established and successively utilized for the calculation of surface exposure ages for individual landforms. The chronological investigation of development and stabilization of the respective landforms permitted an assessment of Holocene climate variability in Rondane and its impact on overall landform evolution. Our obtained SHD age estimates ranged from 11.44 ± 1.22 ka (ST-D2) to 4.09 ± 1.51 ka (AF1) showing their inactive and relict character. Most surface exposure ages for sorted stripes clustered between 9.88 ± 1.35 ka and 9.25 ± 1.21 ka, hence indicating stabilization during the late stage of the Erdalen Event or shortly thereafter. It is inferred that the blockfield formed prior to the Last Glacial Maximum, was protected by cold-based ice throughout glaciation and shortly reactivated during the Erdalen Event only to subsequently becoming inactive. The surface exposure age of a rock-slope failure (7.58 ± 0.73 ka) falls into the early phase of the Holocene Thermal Maximum (HTM, ~8.0–5.0 ka). This indicates permafrost degradation and/or increasing hydrological pressure negatively influencing slope stability. The paraglacial alluvial fan with its four subsites yielded ages between 8.73 ± 1.63 ka and 4.09 ± 1.51 ka. The old exposure ages point to fan aggradation following regional deglaciation due to paraglacial processes, whereas the younger ages can be explained by increasing precipitation during the onset neoglaciation at ~4.0 ka. Our results underline the importance of meltwater for the activation of periglacial landforms in a continental climate and indicate that the Erdalen Event and immediately following onset of the HTM had major impact on landscape evolution in Rondane. Our obtained surface exposure ages from boulder-dominated landforms in Rondane give important insights into the local palaeoclimatic variability during the Holocene.

1. Introduction

Boulder-dominated periglacial and paraglacial landforms are widespread in mid- and high-latitudinal mountain regions worldwide (Ballantyne and Harris, 1994; Ballantyne, 2018; French, 2018). Reconstructing their age and origin as well as exploring their morphodynamics are important for improving our understanding of the controlling mechanisms for landform evolution under past climatic conditions given their development is often related to cold climate-related factors such as freeze-thaw processes and/or the presence of permafrost (Washburn, 1956, 1979; Wilson and Matthews, 2016; French, 2018; Marr et al., 2019c; Wilson et al., 2020; Winkler et al., 2021). Paraglacial landforms can help to assess frequency and magnitude landscape responses conditioned by the paraglacial adjustment

* Corresponding author at: University of Vienna, Department of Geography and Regional Research, Geomorphological Systems and Risk Research, Universitätsstraße 7, 1010 Wien, Austria.
E-mail address: philipp.marr@univie.ac.at (P. Marr).

https://doi.org/10.1016/j.geomorph.2022.108251
Received 21 October 2021; Received in revised form 8 April 2022; Accepted 8 April 2022
Available online 12 April 2022

phase following deglaciation (Church and Ryder, 1972; Ballantyne, 2002; Kerguillec and Sellier, 2015; Matthews et al., 2020b). Providing surface exposure ages of peri- and paraglacial landforms allows building a geochronological basis for their development and final stabilization as well as utilizing them as palaeoclimatic archives (Whittecar and Ryter, 1992; Shakesby et al., 2006, 2020; Matthews and Winkler, 2011; Winkler et al., 2016, 2020; Marr et al., 2018; Wilson et al., 2020).

Major obstacles with the palaeoclimatic interpretation of boulder-dominated peri- and paraglacial landforms were often limitations to numerically date them. This is either caused by their diachronous and long-term formation (as opposed to individual, short-term events), or by methodological and financial constraints regarding the application of established dating methods. As a result, dating of boulder-dominated peri- and paraglacial landforms by Schmidt-hammer exposure-age dating (SHD) has recently gained attention and subsequently improved our knowledge about their age, origin and morphodynamics (Shakesby et al., 2006, 2011; Matthews et al., 2011, 2014, 2020b; Rode and Kellerer-Pirklbauer, 2011; Wilson and Matthews, 2016; Marr et al., 2019a; Winkler et al., 2020). One prerequisite of applying SHD is to establish a calibration curve based on young and old control points of known age and obtained from similar or comparable lithologies. SHD has meanwhile proven to be a valuable method in various geomorphologic circumstances, such as moraines (Winkler, 2014; Tomkins et al., 2018), alluvial fans (Matthews et al., 2020b), rock glaciers (Matthews et al., 2013; Winkler and Lambiel, 2018; Nesje et al., 2021), snow avalanche boulder fans (Matthews et al., 2020a), patterned ground (Winkler et al., 2016, 2020; Wilson et al., 2017; Marr et al., 2018) and rock-slope failures (Matthews et al., 2018; Marr et al., 2019a).

Numerous studies investigating Holocene climate change have been carried out in South Norway (Nesje et al., 1991; Nesje and Dahl, 2001; Dahl et al., 2002; Matthews and Dresser, 2008; Nesje, 2009). However, there is a large discrepancy in the number of studies undertaken between the areas west and east of the watershed. Natural environmental change research during the last decades predominantly focused on western South Norway, e.g. Jotunheimen (Matthews, 1987; Nesje et al., 2001; Matthews et al., 2009; Matthews and Owen, 2010; Winkler et al., 2016; McEwen et al., 2020). In contrast, only few studies have been carried out within eastern South Norway, specifically in Rondane (Dahl, 1956; Gehrenkamper and Treter, 1983; King, 1984; Dawson et al., 1986; Shakesby et al., 1987) and particularly investigating climatic variabilities throughout the Holocene (Kvisvik et al., 2015). This is despite the presence of periglacial features (Barsch and Treter, 1976; Kerguillec and Sellier, 2015; Sellier and Kerguillec, 2021) and the ideal properties to investigate geomorphological processes due to the homogeneous lithological structure (Strøm, 1945). This unexplored potential for investigating periglacial and related landforms as palaeoclimatic indicators may provide relevant insights into landscape transition following deglaciation. These results can be valuable for better understanding about the timing and magnitude of Holocene cold climate periods and the response of geomorphological systems to these in a continental setting in comparison to the better studied maritime environments in western South Norway.

In this paper, we assess the applicability of SHD in Rondane, South Norway for the first time, for investigating age and origin of peri- and paraglacial landforms. To improve our understanding of their conditioning by Holocene climate fluctuations we investigate sorted stripes (ST), a blockfield (BL), a rock-slope failure (RSF) and an alluvial fan (AF). The obtained age constraints are interpreted and discussed within the context of Holocene climate fluctuations in South Norway. Our three main objectives are as follows: (i) to establish the first SHD calibration curve in Rondane, (ii) to determine the timing of formation and stabilization of boulder-dominated landforms with SHD, and (iii) to relate landform evolution to changing climatic conditions during the Holocene.

2. Study area

2.1. Location, geological and geomorphological context

The Rondane mountains, located in eastern South Norway (Fig. 1) are part of the Scandinavian Caledonides (Oftedahl, 1950; Ramberg et al., 2008). They cover an area of about 2030 km^2 with several peaks above 2000 m a.s.l., the highest peak is Rondslottet 2178 m a.s.l. (Strøm, 1945; Shakesby et al., 1987). The gross morphology of Rondane is characterized by near-horizontal plateaus, wide transactional valleys, numerous peaks above 2000 m a.s.l., glacial cirques and few glacial troughs. The geomorphological map of Rondane (Barsch and Treter, 1976) displayed a large variety of periglacial and related landforms, both active and relict. Talus-covered slopes and boulder-dominated landforms are the result of steep valleys, jointed rock structures, freeze-thaw activity and relatively low fluvial erosion in the upper valley parts (Shakesby et al., 1987). Patterned ground cover, such as sorted stripes, was reported between 1250 and 1700 m a.s.l. (Barsch and Treter, 1976). Additionally, lateral drainage channels are abundant features (cf. Kvisvik et al., 2015). In this study, we focus on two areas in Rondane, namely Fremre in the south and Haverdalen in the north (see Fig. 1) Geomorphological details surrounding the specific landforms are described in Section 3.2.

Geologically, the bedrock in Rondane is dominated by quartzite rocks. The area consists mainly of feldspathic sandstone, named arkosic sparagmite (Oftedahl, 1950). It is partly constituted of meta-sandstone and conglomerates with a relatively high quartz and feldspar content (Strøm, 1945; Sigmond et al., 1986). Both areas in Rondane mainly consist of metasandstone with quartzite as an additional rock type (Tveten et al., 1998). In the more detailed geological map 1:50,000 (www.ngu.no – Geological Survey of Norway/www.ngu.no, 2022), the area around Fremre is characterized by sandstone whereas Haverdalen consists of meta-arkose.

2.2. Climate, permafrost and palaeoclimate

The climate conditions in Rondane can be described as “dry periglacial”(Sellier and Kerguillec, 2021), and are characterized by relative continentality. Mean annual temperatures vary from −6 to 0 °C (1971–2000) in the entire Rondane area (www.senorge.no, 2020), and winter precipitation estimates (1 October–30 April) based on data from climate stations at Fokstua (974 m a.s.l.), Folldal (709 m a.s.l.) and Høvringen (935 m a.s.l.) give on average 176 mm w.e./a at 1000 m a.s.l. (www.met.no). The mean number of days with snow depth of >25 cm is 200–350 for most of the study area, but sites in Haverdalen (AF, RSF) experience snow depth of >25 cm for only 100–200 days (www.senorge.no). According to Bjørbæk (1993), snow-bearing winds from southwest are dominant during winter and result in higher local leeward accumulation of snow and limited snow cover on summits.

The permafrost distribution in the Rondane massif is of considerable size (Gisnås et al., 2013, 2017), however, there are no detailed recent data available concerning ground temperatures. In proximity to the study area on Blåhø/Jetta (ca. 25 km west of Rondvassbu) an array of three permafrost boreholes at 1218 m a.s.l., 1450 m a.s.l. and at 1560 m a.s.l. was installed (Farbrot et al., 2011). At the uppermost borehole marginal permafrost was detected (Farbrot et al., 2011), in general above 1500 m a.s.l. permafrost conditions can be assumed (Etzelmüller et al., 2003). The lowest situated rock glacier in Rondane is located at ~1500 m a.s.l. where also the present limit of discontinuous permafrost is expected (Lilleøren and Etzelmüller, 2011). According to Isaksen et al. (2007) the present permafrost limit is most likely located above ~1450 m. Except for the Skriufonne cirque glacier, there are currently no glaciers in Rondane (Kvisvik et al., 2015).

The Rondane massif is located north of the main ice divide in southern Norway during the last glacial maximum (LGM) (e.g. Dahl et al., 1997, and references therein), and low-erosive cold-based ice

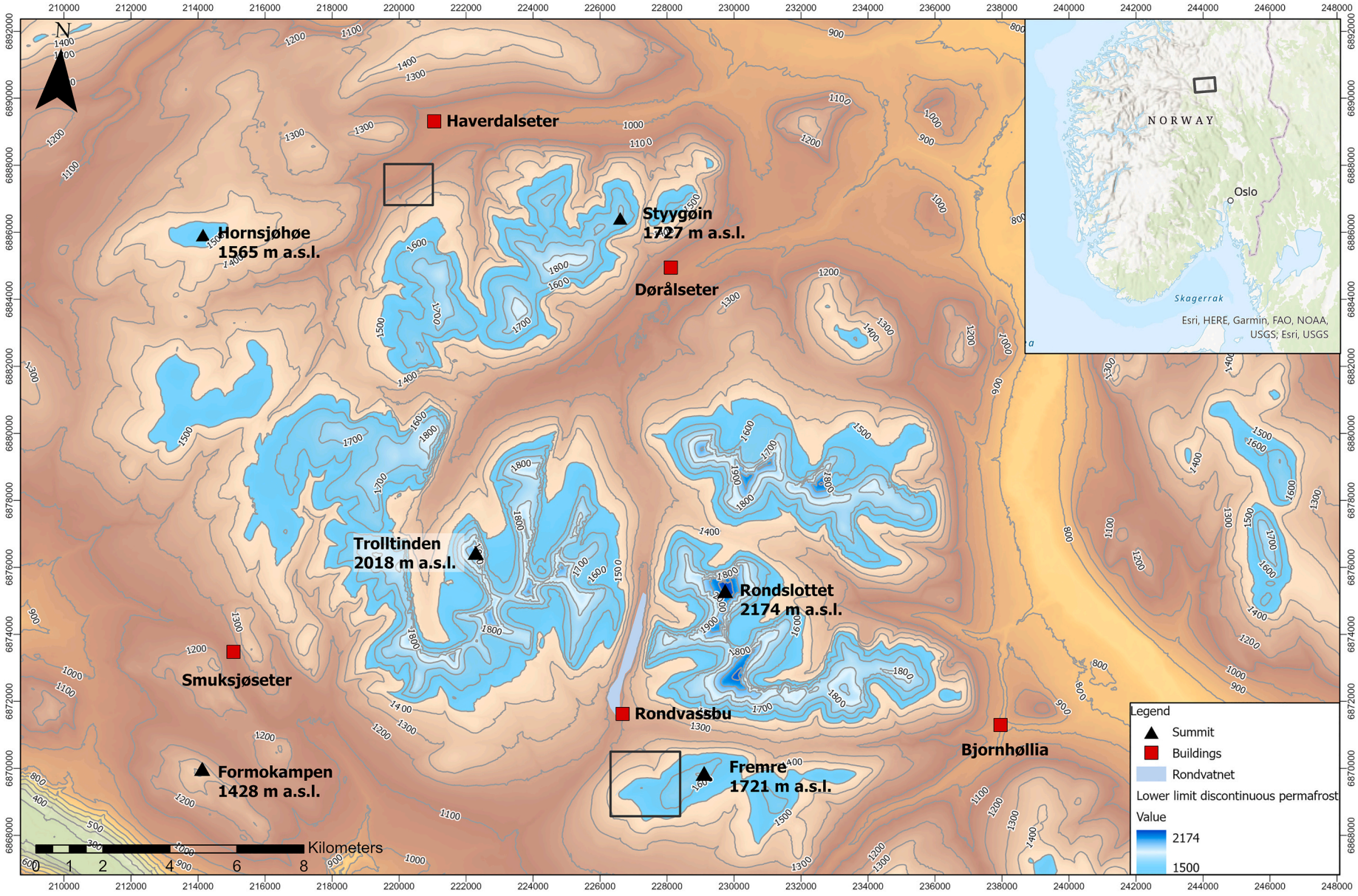

Fig. 1. The Rondane massif, South Norway with two black squares indicating the areas of geomorphological features selected for SHD (© Kartverket/www.kartverket.no).

conditions are suggested for the Rondane area during this period (e.g. Sollid and Sørbel, 1994; Dahl et al., 1997; Patton et al., 2016). The few glacial troughs in the valleys contrast the well-developed cirques are suggested to be the result of cold-based ice sheets during major glaciations and warm-based and/or polythermal cirque glaciers during interglacials or interstadials (Dahl et al., 1997; Kleman, 2008). The timing of final deglaciation in the area was estimated to ~10 ka based on the compilations of regional chronologies by Hughes et al. (2016), and Stroeven et al. (2016), and Kvisvik et al. (2015) suggested that a rapid local deglaciation occurred during the early-Holocene in central Rondane at around 10 ka. Permafrost conditions probably survived the deglaciation in most parts of Rondane and remained present at higher elevations throughout the Holocene (Lilleøren and Etzelmüller, 2011; Lilleøren et al., 2012). However, permafrost is suggested to have partly degraded during the Holocene Thermal Maximum (HTM, ~8.0–5.0 ka, Clark et al., 2009) (Lilleøren and Etzelmüller, 2011; Lilleøren et al., 2012). Following the Finse Event (equivalent of the 8.2 ka Greenland event), the HTM in Norway most likely resulted in the disappearance of all glaciers in Norway (Nesje, 2009). However, the local Late Pleistocene and Holocene glaciation history in Rondane is relatively poorly explored.

3. Methodology and research design

3.1. Geomorphological measurements, clast roundness and palaeohydrological indicators

Landforms integrated in this study were identified based on aerial photography, geomorphological maps (Barsch and Treter, 1976) and by field investigations in summer 2020. We aimed to sample different peri- and paraglacial landforms in Rondane in order to better understand their responses to climatic variations. Topographic (elevation, aspect, slope angle) and geomorphologic information were gathered in the field and validated with topographic and geomorphologic maps. The measurements of lengths and widths of landforms and boulders were performed in the field with measuring tape.

Determining the roundness of a minimum of 25 representative boulders at each landform was based on the visual comparison method introduced by Powers (1953). Clast roundness provides indications about transporting trajectories of boulder accumulations on the alluvial fan (Matthews et al., 2020b) or potential effects on R-values and sorted stripe morphology (Winkler et al., 2020). The roundness index of mean roundness was applied ranging from very angular 0.5, angular 1.5, …, to well-rounded 5.5 (Powers, 1953).

Palaeohydrological parameters helped to determine the processes and forces which are needed, e.g. to mobilize a certain volume of mass. Following Matthews et al. (2020b), the intermediate-(b-axis) were measured from the boulder deposits on the alluvial fan in order to calculate palaeohydrological parameters which could be related to the processes involved in sediment deposition (Williams, 1983). In addition to the averaged values of measured boulders, the maximum intermediate-(b-axis) from each site was measured in order to calculate maximum values. The palaeohydrological parameters were estimated from the intermediate-(b-axis) clast size (d) (Williams, 1983):

$$\text{Unit stream power } (\omega) = 0.079\mathrm{d}^{1.3} (10 \leq \mathrm{d} \leq 1500 \text{ mm}) \quad (1)$$

$$\text{Bed shear stress } (\tau) = 0.17d^{1.0} (10 \leq \mathrm{d} \leq 3300 \text{ mm}) \quad (2)$$

$$\text{Mean flow velocity } (\mathrm{V}) = 0.065d^{0.50} (10 \leq \mathrm{d} \leq 1500 \text{ mm}) \quad (3)$$

3.2. Investigated landforms

Owing the dry periglacial climate and the geological properties, the Rondane mountains comprise a variety of periglacial and related landform assemblages (e.g. Barsch and Treter, 1976). These include sorted stripes, a blockfields, a rock-slope failure and boulder accumulations on an alluvial fan (Figs. 2a, b, 3), most of which are associated with past periglacial and/or permafrost conditions (Ballantyne, 2018; French, 2018). All landforms share a relict character with no evidence of recent, post-depositional disturbance.

Sorted stripes were sampled in South Rondane from the southwest to north around the Fremre summit (Figs. 2a, 3). In total, four sorted stripe clusters (A-D) were investigated, each subdivided into upper (ST-A1, ST-B1, …) and lower (ST-A2, ST-B2, …) segments. Each segment consisted of four individual stripes, measured with 100 impacts for each stripe including the upper and lower part. The stripes were selected in varying aspects, southwest (ST-A1, ST-A2, ST-B1, ST-B2), west (ST-C1, ST-C2) and north (ST-D1, ST-D2) at an elevation between 1338 (ST-C2) and 1551 m a.s.l. (ST-A1). The slope angles varied between 6° and 20°. The average boulder size within the sorted stripes 20–45 cm, dominated by subangular clasts. The stripe widths ranged from 50 to 350 cm with an average of ~150 cm, the width of the fine-grained area separating them ranged between 70 and 420 cm, averaging to ~200 cm. The length varied between ~35–100 m. Whereas, the largest width was observed in the upper slope area, other stripes also had large widths at their downslope terminus. Whereas some stripes were parallel aligned with slope inclination, others showed curve-like patterns.

The area of our investigated blockfield (BL; $n = 400$; N61°51′28.7″, E9°47′57.2″; 1480 m a.s.l.) comprised ~5000 m^2 and is located west of the Fremre summit in the southern part of Rondane, close to Rondvassbu (see Figs. 2a, 3). In total, four subsites (every 200 m along a northeast transect) with 100 boulders each were measured. Generally, the blockfield is characterized by smaller topographic variations and boulder tongues indicating (past) downslope movement by solifluction. Partly, the lobes showed signs of soil matrix and vegetation. The entire slope gradient averaged at ~15°, with steeper parts towards the summit. Surface depth was 15–40 cm with an average boulder diameter ranging from 40 to 60 cm.

Our investigated rock-slope failure (RSF; $n = 500$; N62°01′16.7″, E9°38′23.8″; 1060 m a.s.l.) in North Rondane (Figs. 2b, 3) had a total area of about 9300 m^2 and the southeast exposed slope had an angle of ~14°. The entire slope was characterized by boulders with an average size between 30 and 60 cm, with largest boulder with a diameter of 120 cm. The scar upper part of the slope was clearly visible, the area underneath was dominated by birch trees and at the foot of the slope a parallel oriented ridge was limiting the run-out zone of the boulders. The landform surface had depressions and rises as well as varying slope inclination. Some boulder accumulations were concentrated between vegetated ridges.

Moreover, we investigated a relict paraglacial alluvial fan (AF; $n = 400$; N62°01′12.8″, E9°39′00.9″; 1050 m a.s.l.) at the opposite side of RSF on the valley floor of Haverdalen with an area of 110,000 m^2. Paraglacial alluvial fans were particularly observed in the northern part of Rondane (Kerguillec and Sellier, 2015) where the AF of this study was located. The fan catchment was currently not glacierized. The fan lied at the foot of a mountain ridge of ~1700 m a.s.l. which was expected to have been affected by glaciation during past glaciations. In total, four locations each with 100 boulders were sampled in different parts of the fan (Figs. 2b, 3, 4). The boulder deposits on the fan showed different shapes from widespread accumulation (AF1, AF2), an irregular ridge (AF3) and regular ridge (AF4; ~80 m length). The slope angle at the four sample sites generally varied between 5° and 10° with an exceptional steep distal lobe of 20° at AF3. Average boulder sizes varied from 30 to 50 cm.

3.3. Schmidt-hammer readings

The Schmidt-hammer rebound measurements (R-values) were carried out on 14 boulder-dominated landforms. All measurements were obtained in dry conditions by a single operator with a N-Type electronic RockSchmidt (Proceq, 2014). The hammer was calibrated before and

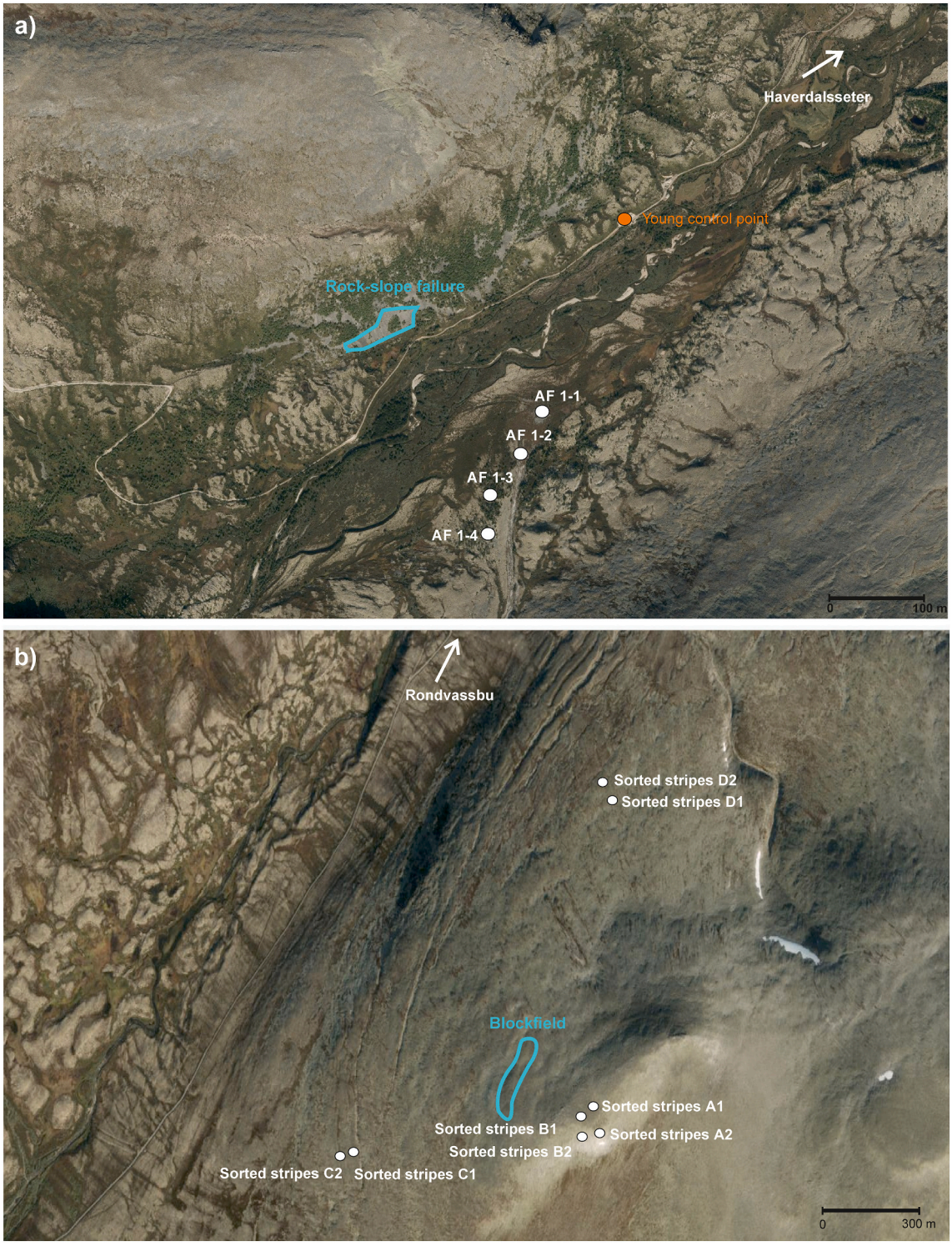

Fig. 2. Aerial photos of the investigated landforms (a) in Haverdalen, North Rondane and (b) around Fremre in South Rondane. Aerial photography adapted from www.norgeibilder.no, © Kartverket/www.kartverket.no.

after the field survey on the manufacturers test anvil, no deviations from the calibration standard were noted. Individual boulders were randomly selected and only stable boulders with an average long axis between 30 and 50 cm were measured. Readings were derived from lichen-free boulder surfaces, whereas corners, visible cracks or lithological weaknesses were avoided. The few lichen-free spots were preferably sampled and, if small bits of lichen thalli were protruding into the small spots required for the plunger, it was ensured that these are crustose lichens and will (if at all) only marginally influence the R-values by potentially slightly lowering them. Rock surfaces were not prepared or modified before measurement (see Matthews et al., 2015).

Here, we measured a minimum of 100 boulder surfaces at each landform. Boulder samples were obtained with one impact. This sampling design was similar to that applied by SHD studies on similar landforms (e.g. Wilson et al., 2020; Winkler et al., 2020). The collected R-values from each landform were initially treated as one statistical

Fig. 3. (a) View on the alluvial fan (AF1) towards south. (b) View of the blockfield towards north to Rondvassbu which is located at the front tip of the lake. (c) In the foreground alluvial fan site (AF4) with the rock-slope failure in the background. (d) Sorted stripe (ST-A2) at Fremre with view towards northeast. The pole is 1 m long.

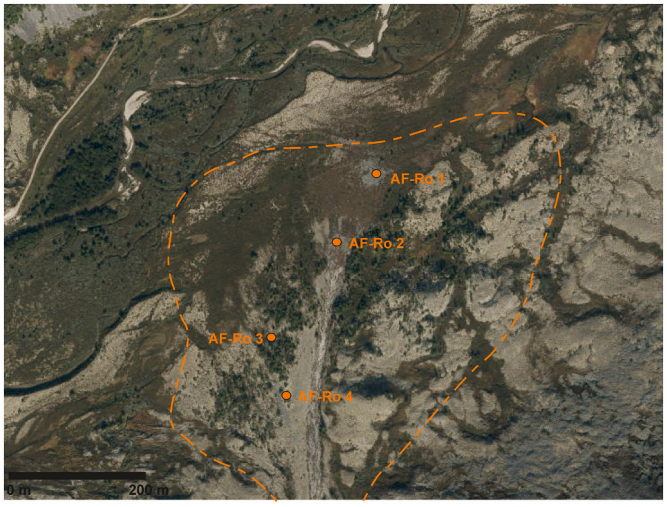

Fig. 4. Aerial photograph of the alluvial fan showing the numbered subsites and the fan outline. Aerial photography adapted from www.norgeibilder.no, © Kartverket/www.kartverket.no.

population. Mean R-values and the 95% confidence interval ($\alpha = 0.05$), were calculated applying standard statistical analyses (for details see Shakesby et al., 2006). Additionally, histograms were produced to present the R-value distributions and surface exposure age estimates were calculated on the basis of two control points of known age (Matthews and Winkler, 2011; Matthews and Wilson, 2015).

3.4. Control points and Schmidt-hammer exposure age dating (SHD)

In order to estimate the surface exposure ages of the selected landforms, the calculation of a local calibration curve with control points of known age (young and old) is necessary. The young control point was obtained from a road cut in Haverdalen with the dominant lithology present in the study area (Figs. 2, 3). The young control point sample (YC; $n = 200$; N62°01′31.8″, E009°39′14.6″; 1036 m a.s.l.) was derived from 'freshly' excavated boulders which did not show signs of any lichen cover. Inspection of aerial pictures (www.norgeibilder.no – open portal of Kartverket/www.kartverket.no, 2020) shows that this road cut exists since at least 1980, but the current boulder accumulation cannot be identified. In the consecutive aerial image from 2009 boulders are present at the current location. Therefore, we estimated that the boulders were exposed during this time and assign an average age of 25 years to YC.

Due to the lack of numerical landform ages in Rondane, data from an old control point from the nearby summit of Blåhø from Marr et al. (2018) were utilized. The obtained old control point (R-value: 49.7 ± 0.92) was derived from a surface previously dated to 11.7 ± 1.0 ka with cosmogenic nuclides by Goehring et al. (2008). As Marr et al. (2018) used the same electronic Schmidt hammer as in this study, no corrections of the R-values were required, which is necessary when different hammer types are applied (see Winkler and Matthews, 2014). The quartz-rich Precambrian bedrock at Blåhø, which are also prevailing in Rondane, are dominated by meta-conglomerate and metasandstone (Tveten et al., 1998). The rock types for the old and young control point as well as for the investigated landforms are generally dominated by quartz-rich material. Matthews et al. (2016) point out that weathered bedrock in South Norway with age of ~10 ka show similar characteristics for the application of SHD, regardless of certain rock types. Therefore, no major influence on the reliability of the landform estimations was expected. The applicability of an N-Type Schmidt hammer within comparable lithologies was shown by Niedzielski et al. (2009) and Matthews et al. (2016).

Calculating the SHD-calibration equation followed the standard procedure (e.g. Matthews and Owen, 2010; Matthews and Winkler, 2011). A linear relationship between R-values and age throughout the Holocene is well established (Shakesby et al., 2011), particularly in periglacial environments with resistant bedrock (Colman, 1981;

Nicholson, 2008). This is sustained by numerous studies (e.g. Wilson and Matthews, 2016; Winkler and Lambiel, 2018; Marr et al., 2019a). For the calibration curve, a standard linear regression was applied:

$$y = a + bx \tag{4}$$

where y is the surface age in years, a is the intercept age, b is the slope of the calibration curve and x is the mean R-value. The b coefficient is described as:

$$b = (y_1 - y_2)/(x_1 - x_2) \tag{5}$$

with y_1 and x_1 representing the age and mean R-value of the old control point, and y_2 and x_2 of the young control point. By substitution in the calibration equation, the b coefficient was calculated.

The confidence interval for the SHD age represented the total error (C_t), consisting of the error of the calibration curve at the point related to the sampled surface (C_c) and the error of the sample itself (C_s):

$$C_t = \sqrt{(C_c^2 + C_s^2)} \tag{6}$$

The calibration curve error is reflected by the errors of the control points and their age differences:

$$C_c = C_o - \left[(C_o - C_y)(R_s - R_o)/(R_y - R_o) \right] \tag{7}$$

with C_o expressing the 95% confidence interval of the old control point in years, C_y the 95% confidence interval of the young control point in years. R_o, R_y and R_s are associated to the mean R-value of the old and young control point and the sample. The sampling error of the sample itself was calculated incorporating the b coefficient, Student's t statistic, standard deviation (s) of the sample's R-value and the sample size (n):

$$C_s = b[ts/\sqrt{(n-1)}] \tag{8}$$

4. Results

4.1. Schmidt hammer R-value measurements

The results of the Schmidt hammer readings of the control sites are displayed in Table 1. The young control point yields a mean R-value of 72.1 ± 0.86 compared to values from the old control point of 49.7 ± 0.92 reported by Marr et al. (2018). The slightly higher 95% confidence interval of the old control point is often related to longer surface exposure and subaerial weathering leading to more pronounced lithological differences between individual boulders or the effect of an increased micro-topography of the surfaces (Winkler and Matthews, 2014). The calibration curve based on these data was calculated to y = 37,603.906–521.20536x.

The R-values of the investigated landforms were summarized in Table 2. All R-values were located between the values of the young and old control point. The landforms failed the Shapiro-Wilk test for normality except for ST-D2, share negative skewness and alternating kurtosis distributions. The mean R-values with 95% confidence interval ranged from 50.22 ± 1.89 for ST-D2 to 64.3 ± 2.42 for AF1. The 95% confidence interval was largest at AF3 and lowest at RSF. Generally, the 95% confidence intervals and standard deviations were slightly higher compared to other SHD studies (e.g. Wilson and Matthews, 2016; Matthews et al., 2020b). Most sorted stripe sites showed a rather narrow range of mean R-values between 53.2 and 54.4, except for ST-D2 with 50.2. The mean R-values of the sorted stripes samples did not show any significant difference between the upper and lower lying sampling locations. Additionally, no relationship between R-value and elevation was detected. The mean R-values of the alluvial fan sub-sites showed largely overlapping 95% confidence intervals except for AF1 which did not overlap with AF3 and AF4.

Table 2
Schmidt hammer R-values, standard deviation, kurtosis, skewness and n for the studied landforms.

Site	Mean ± 95% CI[a]	σ	Kurtosis	Skewness	Boulders (n)
AF1	64.3 ± 2.42	12.19	−0.55	−0.62	100
AF2	61.0 ± 2.21	11.16	0.13	−0.78	100
AF3	56.7 ± 2.85	14.35	−0.46	−0.34	100
AF4	55.4 ± 2.63	13.27	−0.5	−0.32	100
BL	55.6 ± 1.16	11.83	0.44	−0.55	400
RSF	57.6 ± 0.95	10.8	0.3	−0.66	500
ST-A1	53.6 ± 1.85	13.24	−0.4	−0.42	200
ST-A2	54.0 ± 1.86	13.31	−0.35	−0.41	200
ST-B1	54.0 ± 1.72	12.38	−0.4	−0.39	200
ST-B2	53.5 ± 1.77	12.67	−0.08	−0.33	200
ST-C1	53.4 ± 2.35	16.88	−0.73	−0.38	200
ST-C2	53.2 ± 2.14	15.36	−0.46	−0.28	200
ST-D1	54.4 ± 1.87	13.38	−0.07	−0.48	200
ST-D2	50.2 ± 1.89	13.57	−0.22	−0.31	200

[a] Mean of R-values with 95% confidence intervals (α = 0.05).

The frequency distributions of the landforms are shown in Fig. 5. Some histograms display a rather uniform distribution showing a tail with one peak (BL, RSF). The sorted stripes as well as the subsites of the alluvial fan mostly show comparable platykurtic distributions, partly with polymodal characteristics. Most frequency distributions have boulders with low R-values within the population indicating the presence of more weathered boulders.

4.2. Clast roundness and palaeohydrological indicators

The mean boulder roundness for the boulder deposits on the alluvial fan and the sorted stripes are displayed in Table 3. All fan values are characterized by subangular clasts, which is also applicable for most sorted stripe sites, except for ST-A1 showing mostly angular clasts.

Results from the maximum boulder size and the median size (d_{10}) of the 10 largest boulders (d_{max}) were measured at the alluvial fan sites (Table 4). The maximum boulder size ranged from 2.15 m at AF2 to 1.35 m at AF4. The d_{10} was largest with 1.12 m at A1 and lowest at AF4 with 0.93 m. The lowest stream power unit for entrainment (ω) for the largest clasts in the alluvial fans ranged between 927 W m^{-2} (AF4) to 1697 W m^{-2} (AF2) where the AF2 value is comparable to those obtained by Matthews et al. (2020b). Bed shear stress (τ) varied between 230 N m^{-2} (AF4) and 366 N m^{-2} (AF2) for the largest clasts. The calculated mean flow velocities range from 3.0 m s^{-1} (AF2) to 2.4 m s^{-1} (AF3, AF4).

4.3. SHD landform ages

The SHD ages with 95% confidence interval were obtained from the calibration curve based on the mean R-values of the different boulder-

Table 1
Schmidt hammer R-values and statistics for the control sites. Mean R-values were obtained from the means of one impact per boulder, 95% confidence intervals were calculated from the number (n) of sampled boulders.

Control point	Age (in yr)[a]	R-value[b]	σ	95% CI[c]	Kurtosis	Skewness	Boulders (n)
Young	25 ± 10	72.1	6.16	0.86	−0.25	−0.60	200
Old	11,700 ± 1000	49.7	9.34	0.92	−0.31	−0.37	200

[a] Age of the young control point from field observation. Old control point age from (Goehring et al., 2008).
[b] R-values of the old control point obtained from (Marr et al., 2018).
[c] Mean of R-values with 95% confidence intervals (α = 0.05).

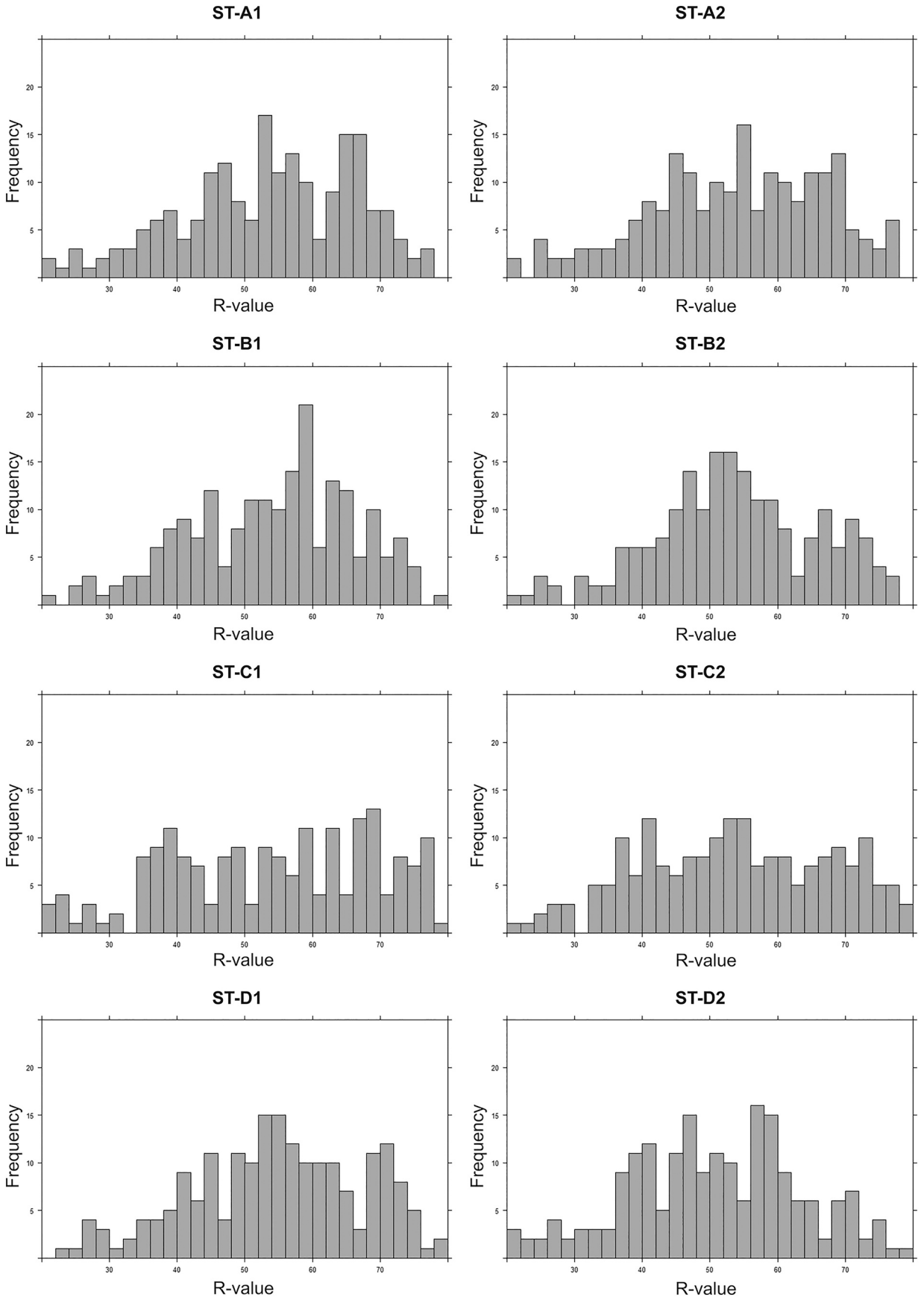

Fig. 5. Frequency distributions of Schmidt hammer R-values from all investigated landforms. Note the different scales for each landform assemblage.

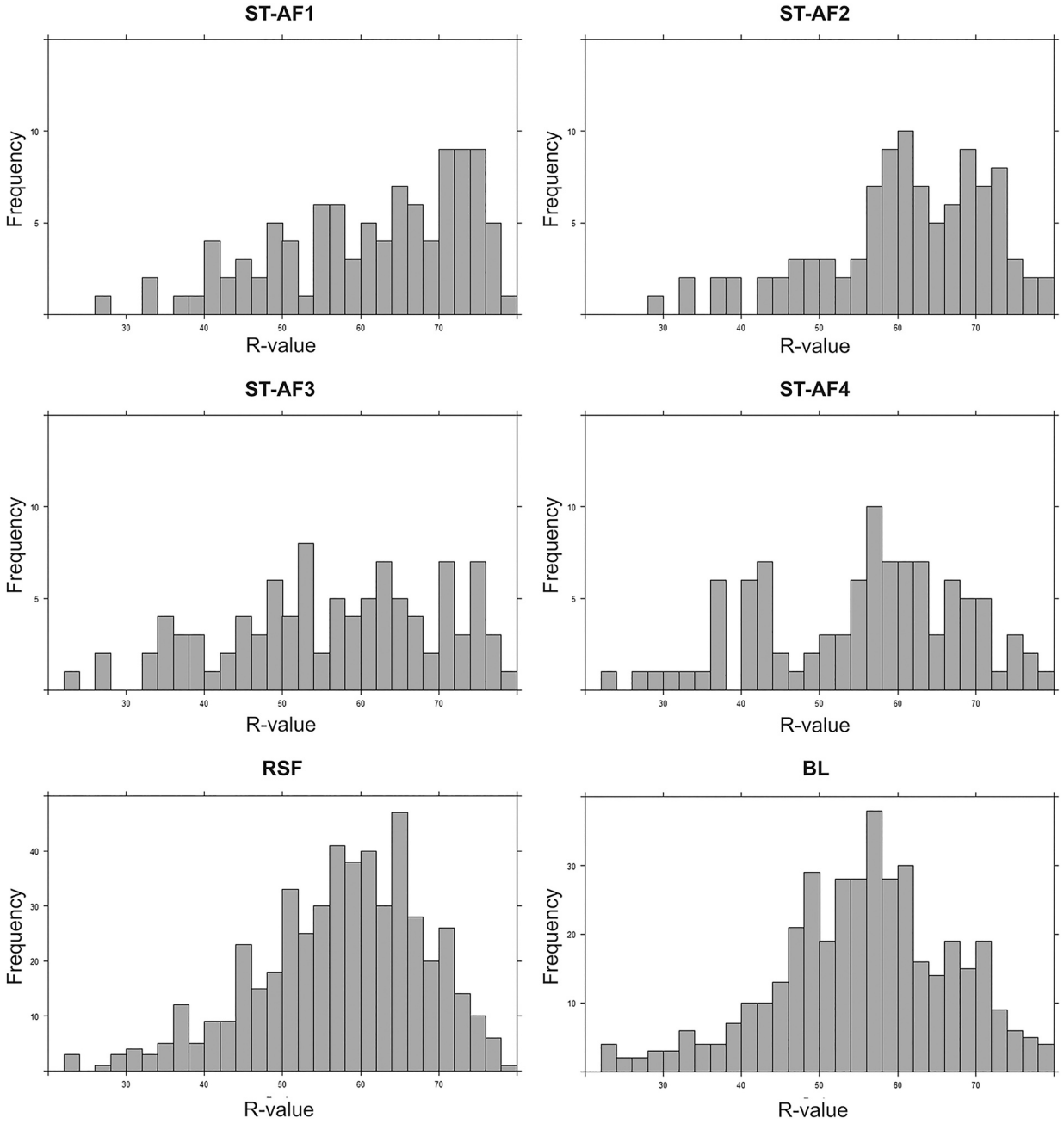

Fig. 5. (*continued*).

dominated landforms (Table 5). The estimated ages range from 11.44 ± 1.22 ka (ST-D2) to 4.09 ± 1.51 ka (AF1). The ages of the sorted stripes are clustered between 9.88 ± 1.35 (ST-C2) and 9.25 ± 1.21 ka (ST-D1), only ST-D2 displayed an older age with 11.44 ± 1.22 ka. As all investigated sorted stripes overlap with the 95% confidence interval (except for ST-D2) and are not significantly different from each other. Therefore, we assume that all sorted stripes stabilized during the same time period. The average sorted stripe sample age is 9.83 ka, excluding ST-D2 the average age is 9.6 ka. Regardless of the mentioned differences, the sorted stripes date to the early-Holocene. The alluvial fan site ages show largely overlapping 95% confidence intervals whereas site AF1 does not overlap with AF3 and AF4 and represent significantly different age populations.

5. Discussion

Previous studies have deciphered block-dominated landforms in the context of the climatic conditions during formation and their development regarding boulder surface weathering differences and hardness (see Wilson et al., 2008, 2020; Kłapyta, 2013; Tomkins et al., 2016). However, the interpretation of SHD ages from diachronous periglacial and paraglacial landforms, including patterned ground features such as sorted stripes, is not a trivial task (Winkler et al., 2016; French, 2018), especially in comparison to landforms representing individual, relatively short-lived events such as moraines (Matthews and Winkler, 2011). This is related to the relatively long formation histories where post-depositional disturbance and various time periods of burial and exposure are considered to be important factors in landform evolution (e.g. Winkler et al., 2016). The obtained SHD age estimates average boulder ages at the surface of the individual landform. As the

Table 3
Roundness data of different landforms with the clast roundness index (IR) and the dominant clast roundness category.

	ST-A1	ST-A2	ST-B1	ST-B2	ST-C1	ST-C2	ST-D1	ST-D2	AF1	AF2	AF3	AF4
n	200	200	200	200	200	200	200	200	25	25	25	25
IR	1.71	2.29	2.25	2.51	2.84	2.78	2.66	3.07	3.1	3.1	3.34	3.18
Dominant	angular	subangular	subangular	subangular	subangular	subangular	subangular	subangular	subangular	subangular	subangular	subangular

Table 4
Palaeohydrological parameters from different boulder deposits on the paraglacial alluvial fan. See text for equations and details.

	Unit stream power ω (W m^{-2})		Bed shear stress τ (N m^{-2})		Mean flow velocity V (m s^{-1})	
	D_{10}	Max	D_{10}	max	D_{10}	max
AF1	728	1367	191	309	2.2	2.8
AF2	719	1697	189	366	2.2	3.0
AF3	589	900	162	224	2.0	2.4
AF4	577	927	159	230	2.0	2.4

Table 5
SHD ages from the sampled landforms. Each SHD age has a 95% confidence interval (Ct) derived from the sampling error of the landform sample (Cs) and the error of the calibration curve (Cc).

Landform	SHD age (ka)	C_t(ka)
AF1	4.09	1.51
AF2	5.81	1.39
AF3	8.05	1.75
AF4	8.73	1.63
BL	8.63	0.83
RSF	7.58	0.73
ST-A1	9.67	1.19
ST-A2	9.46	1.2
ST-B1	9.46	1.12
ST-B2	9.72	1.15
ST-C1	9.77	1.47
ST-C2	9.88	1.35
ST-D1	9.25	1.21
ST-D2	11.44	1.22

investigated landforms did not show signs of post depositional disturbance or recent activity, we consider the SHD ages to be maximum age estimates of the timing of landform stabilization, i.e. it becoming inactive (Wilson and Matthews, 2016). Negatively skewed R-value distributions of all landforms indicated that some boulders had already been exposed prior to landform stabilization, underlining dynamic landform evolution.

5.1. Methodological considerations

The reliability of the control points and the calculation of the calibration curve are vital for a successful SHD application (Matthews et al., 2014). A potential weakness of the old control point could be its non-local origin, due to the lack of surface exposure ages in Rondane. We adopted R-values from a study by Marr et al. (2018) from the nearby summit of Blåhø with comparable lithology. The application of regional control points in situations with comparable lithologies and surface roughness, these non-local control points appear to have been weaknesses in former studies (Matthews et al., 2011). Obtaining regional rather than local control points in general lowers the precision of the SHD ages. However, due to the general lithological homogeneity in the area (see Section 2.1), the R-value range between the control points is comparable to other SHD studies (e.g. Wilson and Matthews, 2016; Winkler and Lambiel, 2018) as well as the successful application of SHD with non-local old control points (Matthews et al., 2014; Marr et al., 2019a), we consider our approach reasonable. As shown by Matthews et al. (2016) with SHD, weathered bedrock in South Norway with an age of ~10 ka exhibits a similarly high degree weathering irrespective of certain rock types. According to Matthews et al. (2014), compared to statistical and other inaccuracies associated with SHD, the age errors of the control points is regarded as insignificant. With the character of the young control point some uncertainty is related to potential subterrane weathering of the boulders exposed during road construction as discussed by Winkler et al. (2016) in a similar case. Therefore, we consider that our approach produces reliable landform age estimates.

The results presented here mostly showed relatively high standard deviations and 95% confidence intervals in comparison to other studies, e.g. on sorted stripes (Winkler et al., 2020) or alluvial fans (Matthews et al., 2020b). This is most likely caused by the relatively small sample sizes we obtained on most landforms. An alternative explanation could be related to the responsible formation processes with the incorporation of boulders from different ages along the feeding channel of the paraglacial alluvial fans or the sorted stripes. As other studies showed that this number of boulders selected for SHD studies are sufficient (Wilson et al., 2017; Marr et al., 2018), we consider the quality of the ages to be reliable.

5.2. SHD landform age interpretation and palaeoclimatic implications

The age estimates of the landforms investigated in this study ranged from 11.44 ± 1.22 ka (ST-D2) to 4.09 ± 1.51 ka (AF1) which underlines their inactive and relict character which agrees with other comparable landforms in South Norway (Winkler et al., 2016; Marr et al., 2019a; Wilson et al., 2020). The development of patterned ground features such as sorted stripes were strongly related to the presence of permafrost and are products of cold climate (and hillslope) processes (Washburn, 1956; Boelhouwers, 1999; Wilson, 2007). Sorted stripes appeared to be active in cold climates, ceasing in warmer conditions and can develop under long time periods with multiple active phases (Wilson et al., 2008, 2017). Nonetheless, the formation processes were complex as the relationship between potential permafrost conditions (e.g. active layer characteristics) and soil moisture, to highlight just two potential influencing factors (Winkler et al., 2020 and references therein). The complex formation histories of patterned ground (Winkler et al., 2016) were reflected in the relatively wide range of frequency distributions (Fig. 5) which was also reported by Bregman and Knight (2020). This indicates a mixed boulder population within the sorted stripes suggesting a polygenetic development. We could not observe elevational patterns of timing of stabilization of landforms which supports findings from Cook-Talbot (1991) on patterned ground. Winkler et al. (2020) reported elevational patterns, however, these were limited to locations on relatively flat terrain because the altitudinal gradient at steeper slopes was overprinted by other processes such as solifluction or gelifluction.

The mean SHD age of all sorted stripes with 9.6 ka (excluding ST-D2, see Section 4.3) has been interpreted as the timing of landform stabilization and mostly overlap with two intervals of climate cooling and advancing glaciers in South Norway: the two phased Erdalen Event (~10.1–10.0 and ~9.7 cal. ka BP; Dahl et al., 2002) and the Finse Event (~8.5–8.0 cal. ka BP; Nesje, 2009), during which the '8.2 ka event' was recorded in the GRIP and GISP2 Greenland ice-cores (see Nesje and Dahl, 2001; Nesje et al., 2001; Matthews and Dresser, 2008). As there were no significant difference between the SHD ages of the upper and lower parts of the sorted stripes, we infer that all stripes became relict accordingly to their SHD age including their uncertainties (Wilson et al., 2017). The platykurtic distributions as well as the non-increasing exposure ages downslope indicate that the boulders were laterally entrained along the slope rather than introduced upslope and transported further down (Winkler et al., 2020). Consequently, we suggest simultaneous sorted stripes stabilization (see Wilson et al., 2017; Winkler et al., 2020).

The sorted stripe development was most likely initiated rapidly following deglaciation with simultaneously progressing permafrost conditions (Lilleøren et al., 2012), as it was assumed for similar landforms elsewhere in Norway (Winkler et al., 2020). The climate during the first Erdalen Event (~10.1–10.0 cal. ka BP) was characterized by a major in increase in winter precipitation, whereas the second (~9.7 cal. ka BP) showed decreasing summer temperatures in western South Norway (Dahl et al., 2002). This is sustained by Paus et al. (2019) who has detected a distinct and short cold spell at 9.7 ka based on ecological indicators from lacustrine sediments in Dovre. Most likely, freeze-thaw processes and frost-heave of boulders was enhanced during this period (Wilson et al., 2017). Our results indicate a relatively fast development of the sorted stripes within ~400 years following deglaciation (~10 ka) which agrees with findings from Kessler et al. (2001) indicating a formation time of 750 years of sorted circles with a 3.6 m width. Rapid sorted stripes initiation following deglaciation is also documented in the Pyrenees (Feuillet and Mercier, 2012). In a regional perspective the sorted stripes in Rondane seem to have formed rapidly, compared to other development rates of sorted stripes in Jotunheimen (Winkler et al., 2020) with 1.5–2.0 ka or ~5 ka western South Norway (Wilson et al., 2017). This rapid development could be associated with the favorable environmental circumstances, such as periglacial climate conditions, an active layer on permafrost and available fine-grained particles with suitable frost susceptibility. However, possibly areas above 1100 m a.s.l. were ice-free prior to the Younger Dryas (Dahl et al., 1997), opening the possibility for a longer development.

The timing of stabilization can be related to shifting climatic conditions from cold/dry towards warm/wet conditions in the Jostedalsbreen area following the Erdalen Event (Nesje et al., 2001). For the continental setting in Rondane, rather dry conditions were suggested beginning ~9 ka (Kvisvik et al., 2015). Most likely, the lack of moisture supply by precipitation due to the continental climate was compensated by supply from melting processes. These circumstances could have favored a rapid development of the sorted stripes which terminated as the terrestrial moisture supply ceased during the warm phase following the Erdalen Event. Increasing temperatures probably led to a thickening of the active layer and degrading permafrost resulting in a lower frequency and magnitude of freeze-thaw dynamics, due to less favorable soil moisture conditions which are important for freeze-thaw and other processes (Vandenberghe, 1988; Luoto and Hjort, 2004). Lack of fines available for frost processes could also be a way of explaining the ceasing of sorted stripe activity (Ødegård et al., 1988).

There was no evidence of re-activation of the processes at the sorted stripes during later cold events. This could be related insufficient moisture supply for initiating major morphodynamic changes due to the continental setting. The lack of precipitation could not be compensated by terrestrial sources, as limited snow reservoirs in the mountains in proximity to Rondane are inferred by little or no flood activity between 9 and 4 ka (Bøe et al., 2006; Støren and Paasche, 2014). Additional reasons for the prevailing inactive status might be the mature stage of the sorted stripes or that the conditions were fundamentally different from those during their development (see Winkler et al., 2020). Based on these findings and the SHD ages and their uncertainties, we infer that the sorted stripes stabilized during the late stage of the Erdalen Event. The timing of stabilization of sorted stripes is supported by findings from Wilson et al. (2017) in western South Norway with reported sorted stripe ages around ~11.2–7.2 ka. Sorted stripes in Jotunheimen became inactive between ~7.9–6.6 ka (Winkler et al., 2020) following the Finse Event, at the onset of the HTM. Their later stabilization compared to Rondane could be related to higher moisture supply during the Finse Event enabling freeze-thaw processes to work.

The SHD age of the blockfield (8.63 ± 0.83 ka) indicates that it stabilized during the early-Holocene. It is inferred that large parts of the Rondane mountains were covered by cold-based ice during last glaciation (Sollid and Sørbel, 1994; Dahl et al., 1997; Kleman, 2008) which had the potential to maintain blockfield structures (Fjellanger et al., 2006; Fabel et al., 2012; Ballantyne and Stone, 2015). Consequently, it is possible that the initial blockfield age is older than indicated by our SHD ages and that it was laid out prior to the last glaciation. An older age and long-term formation are supported by the negative skewness and the relatively broad confidence interval. This reflects the reactivation of geomorphic processes during cold events which led to enhanced heaving processes where older boulders were re-mobilized (Matthews et al., 2014). The blockfield age is relatively young compared to other numerically dated blockfields in South Norway, as most exposures ages from blockfields are older than 20 ka, possibly date back to the Tertiary (Rea et al., 1996; Linge et al., 2006; Goodfellow, 2012). The blockfields

on Elgåhogna and Blåhø experienced ice-free conditions between 19 and 17 ka or earlier (Goehring et al., 2008; Marr et al., 2018, 2019b). Therefore, we argue that it is unlikely that the blockfield formed in this relatively short time period following deglaciation and inherits a longer history with its initial formation prior to the LGM.

Regardless of the initial blockfield age, it appears that it was active following ice melt-down due to prevailing periglacial climatic conditions in Rondane. The SHD age overlaps with the Erdalen and Finse Event. Two explanations appear possible. 1) The blockfield surface boulders stabilized during the Finse Event, when temperatures were characterized by cold and dry conditions (Nesje et al., 2001). During the 8.2 event, continental climate with enhanced amplitude of seasonal temperatures and colder winters were assumed (Alley and Ágústsdóttir, 2005). Therefore, enhanced freeze/thaw and heaving processes together with drier and windier conditions during colder winters were expected (Alley and Ágústsdóttir, 2005; Wilson et al., 2017) which could be a reason for the reactivation of the blockfield and the relatively young exposure age. 2) The blockfield age was not statistically distinguishable with the sorted stripes indicating they stabilized simultaneously during the Erdalen Event. Additionally, the geomorphological situation on Fremre, the embedding of the blockfield in proximity to the sorted stripes and altitudinal-wise located between ST-A/B and ST-C supports the notion of a similar stabilization timing. Due to the differing formation dynamics of sorted stripes and blockfields it seems unlikely that the more dynamic stripes did not react to a cold climate event whereas the blockfield, usually considered with long-term morphodynamics, reacts. Based on these thoughts, we infer that the blockfield structure was laid out prior to the LGM and protected by cold-based ice. Following deglaciation, the landforms on Fremre stabilized altogether in the late stage of the Erdalen Event.

The estimated age of stabilization of the rock-slope failure debris with 7.58 ± 0.73 ka indicates that the RSF occurred during the early phase of the HTM. The unimodal nature of the histogram as well as the narrow confidence interval supports the notion that the RSF formed during a single event. R-value histograms from other landforms which were formed during one event, such as moraines or RSFs show similar characteristics (Aa and Sjåstad, 2000; Winkler, 2014; Marr et al., 2019a). The reason for the rather broad confidence interval could be the occurrence of consecutive rock falls on the same slope (El Bedoui et al., 2009). The RSF frequency peaks identified by Matthews et al. (2018) at 7.38 ± 0.99 ka as well as the RSF ages reported by Böhme et al. (2015), Marr et al. (2019a), Curry (2021) and Hilger et al. (2021) support the occurrence of RSFs in South Norway characterized by warm climatic conditions during the mid-Holocene and do not necessarily occur rapidly following deglaciation.

The occurrence of rock-slope failures has been connected to different environmental factors such as climate, hydrology and/or geomorphological modifications (Evans and Clague, 1994; McColl, 2012). The transition towards HTM climate was characterized by low winter precipitation and/or higher summer temperatures of about 0.7 °C (Dahl and Nesje, 1996). The progressive warming most likely led to increased freeze-thaw activity, enhanced snow-melt and hydrostatic pressure, decreased permafrost depth all of which might be a mechanism for RSFs (Blikra et al., 2006; McColl, 2012; Ballantyne et al., 2013; Magnin et al., 2019; Etzelmüller et al., 2021). We consider that the complex interplay of the mentioned climatically induced factors together with long-term stress release following deglaciation are responsible for the RSF event (Matthews et al., 2018). Due to the complexity of RSFs it was difficult to determine definite triggers for single events as the mentioned factors are interconnected by different spatial and temporal relationships and feedbacks (McColl, 2012; Ballantyne and Stone, 2013). This together with the regional focus on South Norway led us to embed the RSF age to the new conceptual model that RSF occurrence in Southern Norway are conditioned by Holocene permafrost degradation developed by Matthews et al. (2018).

The chronology of the surface exposure ages of the alluvial fan boulder deposits (Fig. 6) shows that boulders were deposited in the early Holocene between 8.73 ± 1.63 ka (AF4) and 8.05 ± 1.75 ka (AF3), later deposition occurred in the mid-Holocene at 5.81 ± 1.39 ka (AF2) and 4.09 ± 1.51 ka (AF1). The statistically indistinguishable results from most fan subsamples, except for AF1 from AF3 and AF4, complicated the determination of distinct time periods where depositional events such as debris flows occurred.

In comparison to the SHD alluvial fan study by Matthews et al. (2020b) our mean R-values showed relatively high standard deviations and 95% confidence intervals. This and the R-value distributions point to complex formation histories, partly involving consecutive events or reworking of the deposited boulders. According to the attributes compiled by Matthews et al. (2020b), morphological and sedimentologic criteria of the boulder deposits and its characteristics, we assume that debris flows were the dominant flow type. The sediment sources of the fan were most likely located in the upper, steep part of the catchment where unstable sediment was available after deglaciation (Ballantyne, 2002).

Due to the spatial and temporal proximity of AF3 and AF4, we assume that their boulders were deposited around the same time, most likely during the Finse Event. The time lag following deglaciation at AF3 and AF4 could be related to rather late survival of the glacier in the catchment or the changing climatic conditions towards increasing temperatures and precipitation (Matthews et al., 2020b). The occurrence of paraglacial alluvial fans can be explained in the context of the retreat of the LGM ice sheet and thawing permafrost which led to redistribution of sediment and the buildup of alluvial fans (Kerguillec and Sellier, 2015). Additionally, increasing precipitation during the Finse Event was associated with stronger snow-avalanche activity as well as increased flooding events during springtime (Dahl and Nesje, 1996). However, studies in proximity to Rondane indicated generally limited flood activity between 9 and 4 ka pointing to limited snow accumulations in mountainous areas during that period (Bøe et al., 2006; Paasche and Støren, 2014), whereas increasing flood activity was identified with this period between 6 and 4 ka (Vasskog et al., 2011). This might be resolving the SHD ages of AF1 and AF2. The timing of debris flows depositing boulders on AF1, AF2, AF3 and partly AF4 could be explained by generally more mild and wet conditions in South Norway due to a positive NAO index (Nesje et al., 2001). Wetter conditions were favorable for alluvial fan development and our SHD ages could underpin climatic change towards more moist conditions. The combined alluvial fan ages from South Norway showed a frequency peak between 9.7 and 8.0 ka which is termed ‘intense paraglacial aggradation’ period by Matthews et al. (2020b) which coincides with the mean SHD age of AF3 and AF4. They explained this with high sediment availability following deglaciation together with intensified gully propagation.

5.3. Local and regional climatic implications

Rapid disappearance of glaciers in Rondane at ~10 ka occurred slightly earlier than in Jotunheimen at ~9.7 ka (Kvisvik et al., 2015 and references therein). Following the last ice sheet in Rondane, ice thinning progressed and permafrost aggradation within a periglacial climate occurred in the upper slopes, where the sorted stripes started to develop relatively fast. These climatic conditions also re-activated the morphodynamics of the blockfields' surface boulders which most likely formed prior to the LGM. Due to the continental climate, meltwater possibly represented an important share of water, necessary for patterned ground formation and frost heave processes. The formation ceased due to related warming ~8.8 ka (Dahl and Nesje, 1996) and rapid ice wastage following the Erdalen Event (Shakesby et al., 2020), when freeze/thaw and heaving processes were no longer effective. Following the downwastage of glaciers in Rondane, the water supply declined and activity ceased. Notably, the blockfield and sorted stripes from this study stabilized ~9–8 ka later than similar landforms on nearby Blåhø. We explain this with the longer persistence of glaciers or ice accumulations

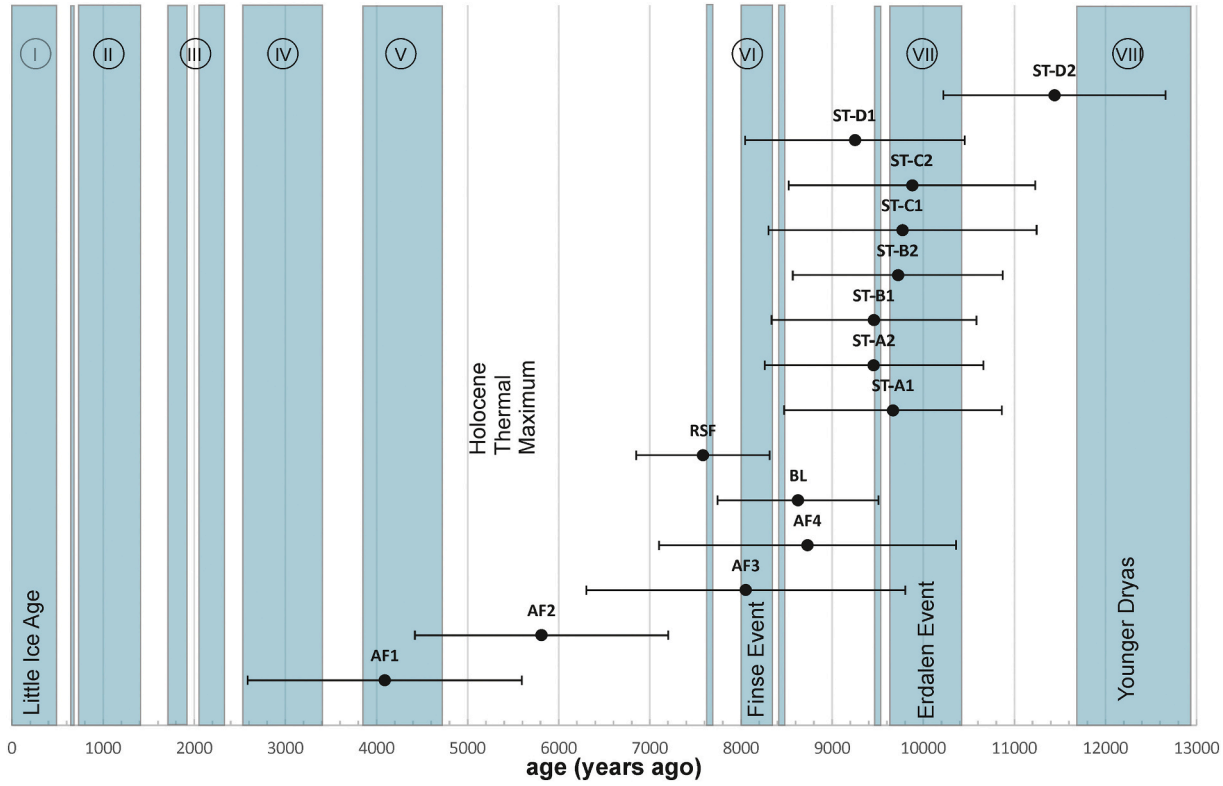

Fig. 6. Plot integrating SHD ages and their total error of the studied landforms in Rondane (AF: alluvial fan; BL: blockfield; RSF: rock-slope failure; ST: sorted stripes). Intervals of documented climatic deteriorations in the Holocene and the Younger Dryas are displayed in roman numbers (Smørstabbtindan I – VII; Younger Dryas VIII). The major climatic deteriorations are displayed in blue bars (Data from Matthews and Dresser, 2008; Lohne et al., 2013). (For interpretation of the references to colour in this figure legend, the reader is referred to the web version of this article.)

in Rondane, glacial meltwater was available which displayed a vital component in the freeze-thaw process system. This underlines the large variety of landform evolution in a spatial limited area. Our results support the notion that the Erdalen Event had strong impact on landform development, as it constitutes the only period within the Holocene where glaciers in South Norway had a larger extent than during the Little Ice Age (e.g. Nesje and Kvamme, 1991; Dahl and Nesje, 1996; Nesje et al., 2001; Dahl et al., 2002). This is sustained by the fact that the sorted stripes where not reactivated during the Finse Event. However, this is in contrast to the findings from Paus et al. (2019) indicating that the Finse Event had a greater impact on shaping landscapes than the Erdalen Event.

The onset of the HTM at ~8 ka together with warmer and wetter conditions progressively weakened permafrost bodies and caused instabilities in the upper slopes (cf. Dawson et al., 1986). Permafrost degradation, which was one of the key drivers of the rock-slope failure can be also related to factors connected to climate amelioration (McColl, 2012; Matthews et al., 2018). The availability of boulder (or till) deposits on steep slopes following deglaciation could have been sensitive to mobilization due to rainstorms or meltwater (Curry, 2000; French, 2018). Wetter and warmer conditions which occurred at the onset of the HTM were possibly also a cause for the occurrence of debris flows depositing boulders on the alluvial fan. All landforms stabilized prior to Neoglaciation and none of the studied landforms were re-activated. This is probably related to the limited moisture supply due to the continental setting in east South Norway, which was also reported from other periglacial and related landforms on Blåhø (Marr et al., 2018). This is notable as starting glacier activity in Rondane ~3.2 ka was documented, lagging behind the Neoglaciation western South Norway (Kvisvik et al., 2015) but did not have detectable effects on the activity of the investigated landforms.

6. Conclusions

This study investigated periglacial and paraglacial landforms in the context of the geomorphological impact of Holocene climate variability in Rondane, South Norway. For the first time in the area, surface exposure ages from different landforms were obtained with Schmidt-hammer exposure age dating (SHD) in order to gain insights into the timing of landform formation and stabilization. We draw the following conclusions:

(i) The electronic RockSchmidt was successfully applied and a calibration curve based on a local young control point of ~25 years and a regional old control point of ~11.7 ka was established. Based on this, reliable SHD landform age estimates were obtained. The SHD ages ranged from 11.44 ± 1.22 ka at a sorted stripe (ST-D2) to 4.09 ± 1.51 ka on boulder deposits on the alluvial fan (AF1).

(ii) Our SHD age estimates indicate that all boulder-dominated landforms stabilized during the early-/mid-Holocene. Most sorted stripes likely formed 400 years following deglaciation. They stabilized in the late phase of the Erdalen Event most likely due to climatic changes and limited moisture supply. Our obtained SHD ages provided the first implications of geomorphic impact of the Erdalen Event in Rondane.

(iii) The investigated rock-slope failure appeared to have occurred during the HTM and not shortly following deglaciation. Most likely, multiple processes associated with warming climate and permafrost degradation led to slope weakening and subsequent failure.

(iv) The formation of the boulder deposits on the paraglacial alluvial fan by debris flows occurred throughout the Holocene in periods

associated with relatively wet conditions and/or snow-melt activity.

(v) Enhanced glacier activity in Rondane and elsewhere in South Norway during the Neoglaciation did not have detectable impact on morphodynamics of the investigated peri- and paraglacial landforms.

(vi) The study shows the importance of the variable the timing of deglaciation in South Norway in rather small spatial distances. It becomes clear that past regional and local climate variability has detectable impacts on geomorphic activity.

(vii) Boulder dominated peri- and paraglacial landforms constitute a valuable source of palaeoclimatic information, geomorphological processes and improve our understanding of Holocene environmental and landscape change.

Funding

This work was supported by a postdoc fellowship of the German Academic Exchange Service (DAAD). The funding source was not involved in study design; in the collection, analysis and interpretation of data.

Declaration of competing interest

The authors declare that they have no known competing financial interests or personal relationships that could have appeared to influence the work reported in this paper.

Acknowledgements

We are thankful to Tabitha Triphaus who contributed during the field work. Additionally, we want to thank two anonymous reviewers for the valuable comments which greatly improved the manuscript.

References

Aa, A.R., Sjåstad, J.A., 2000. Schmidt hammer age evaluation of the moraine sequence in front of Bøyabreen, western Norway. Nor. Geol. Tidsskr. 80, 27–32. https://doi.org/10.1080/002919600750042654.

Alley, B., Ágústsdóttir, A.M., 2005. The 8k event: cause and consequences of a major Holocene abrupt climate change. Quat. Sci. Rev. 24, 1123e1149. https://doi.org/10.1016/j.quascirev.2004.12.004.

Ballantyne, C.K., 2002. A general model of paraglacial landscape response. The Holocene 12, 371–376. https://doi.org/10.1191/0959683602hl553fa.

Ballantyne, C.K., 2018. Periglacial Geomorphology. Wiley Blackwell, Chichester.

Ballantyne, C.K., Harris, C., 1994. The Periglaciation of Great Britain. University Press, Cambridge.

Ballantyne, C.K., Stone, J.O., 2013. Timing and periodicity of paraglacial rock-slope failures in the Scottish Highlands. Geomorphology 186, 150–161.

Ballantyne, C.K., Stone, J.O., 2015. Trimlines, blockfields and the vertical extent of the last ice sheet in southern Ireland. Boreas 44, 277–287. https://doi.org/10.1016/j.geomorph.2012.12.030.

Ballantyne, C.K., Wilson, P., Schnabel, C., Xu, S., 2013. Lateglacial rock slope failures in north-West Ireland: age, causes and implications. J. Quat. Sci. 28, 789–802. https://doi.org/10.1002/jqs.2675.

Barsch, D., Treter, U., 1976. Incidence of periglacial phenomena in Rondane, Norway. Geogr. Ann. A. 58, 83–93.

Bjørbæk, G., 1993. Det norske meteorologiske institutt, vind 1:3,5 mill. Nasjonal atlas for Norge, kartblad 3.1.8. Statens Kartverk.

Blikra, L.H., Longva, O., Braathen, A., Anda, E., Dehls, J.F., Stalsberg, K., 2006. Rock slope failures in Norwegian fjord areas: examples, spatial distribution and temporal pattern. In: Evans, S.G., Mugnozza, G.S., Strom, A., Hermanns, R.L. (Eds.), Landslides from Massive Rock Slope Failure. Springer, Dordrecht, pp. 475–496.. https://doi.org/10.1007/978-1-4020-4037-5_26.

Bøe, A.G., Dahl, S.O., Lie, Ø., Nesje, A., 2006. Holocene river floods in the upper Glomma catchment, southern Norway: a high-resolution multiproxy record from lacustrine sediments. The Holocene 16, 445–455. https://doi.org/10.1191/0959683606hl940rp.

Boelhouwers, J.C., 1999. Relict periglacial slope deposits in the Hex River Mountains, South Africa: observations and palaeoenvironmental implications. Geomorphology 30, 245–258. https://doi.org/10.1016/S0169-555X(99)00033-1.

Böhme, M., Oppikofer, T., Longva, O., Jaboyedoff, M., Herrmanns, R.L., Derron, M.-H., 2015. Analyses of past and present rock slope instabilities in a fjord valley: Implications for hazard estimations. Geomorphology 248, 464–474. https://doi.org/10.1016/j.geomorph.2015.06.045.

Bregman, A., Knight, J., 2020. Analysis of a blockstream in the northern Lesotho Drakensberg, southern Africa. Quat. Int. https://doi.org/10.1016/j.quaint.2020.05.045 (in press).

Church, M., Ryder, J.M., 1972. Paraglacial sedimentation: a consideration of fluvial processes conditioned by glaciation. Geol. Soc. Am. Bull. 83, 3059–3071.

Clark, P.U., Dyke, A.S., Shakun, J.D., Carlson, A.E., Clark, J., Wohlfarth, B., Mitrovica, J. X., Hostetler, S.W., McCabe, A.M., 2009. The last Glacial Maximum. Science 325, 710–714. https://doi.org/10.1126/science.1172873.

Colman, S.M., 1981. Rock-weathering rates as functions of time. Quat. Res. 15, 250–264.

Cook-Talbot, J.D., 1991. Sorted circles, relative-age dating and palaeoenvironmental reconstruction in an alpine periglacial environment, eastern Jotunheimen, Norway: lichenometric and weathering-based approaches. The Holocene 1, 128–141. https://doi.org/10.1177/095968369100100205.

Curry, A.M., 2000. Observations on the distribution of paraglacial reworking of glacigenic drift in western Norway. Nor. Geol. Tidsskr. 54, 139–147. https://doi.org/10.1080/002919500448512.

Curry, A.M., 2021. Paraglacial rock-slope failure following deglaciation in Western Norway. In: Beylich, A.A. (Ed.), Landscapes and Landforms of Norway. Springer, Cham, pp. 97–130.

Dahl, E., 1956. Rondane: mountain vegetation in South Norway and its relation to environment. Skrifterutgittavdet Norske Videnskapsacademii Oslo. Matematisk Naturvidenskapelig Klasse 3, 1–374.

Dahl, S.O., Nesje, A., 1996. A new approach to calculating Holocene winter precipitation by combining glacier equilibrium-line altitudes and pine-tree limits: a case stud from Hardangerjokulen, central southern Norway. The Holocene 6, 381–398. https://doi.org/10.1177/095968369600600401.

Dahl, S.O., Nesje, A., Ovstedal, J., 1997. Cirque glaciers as morphological evidence for a thin Younger Dryas ice sheet in east-central southern Norway. Boreas 26, 161–180. https://doi.org/10.1111/j.1502-3885.1997.tb00850.x.

Dahl, S.O., Nesje, A., Lie, Ø., Fjordheim, K., Matthews, J.A., 2002. Timing, equilibrium-line altitudes and climatic implications of two early-Holocene glacial re-advances during the Erdalen Event at Jostedalsbreen, western Norway. The Holocene 12, 17–25. https://doi.org/10.1191/0959683602hl516rp.

Dawson, A.G., Matthews, J.A., Shakesby, R.A., 1986. A catastrophic landslide (Sturzstrom) in Verkilsdalen, Rondane National Park, Southern Norway. Geogr. Ann. A. 68, 77–87.

El Bedoui, S., Guglielmi, Y., Lebourg, T., Pérez, J.-L., 2009. Deep-seated failure propagation in a fractured rock slope over 10,000 years: the La Clapière slope, the south-eastern French Alps. Geomorphology 105, 232–238. https://doi.org/10.1016/j.geomorph.2008.09.025.

Etzelmüller, B., Berthling, I., Sollid, J.L., 2003. Aspects and concepts on the geomorphological significance of Holocene permafrost in southern Norway. Geomorphology 52 (1), 87–104. https://doi.org/10.1016/S0169-555X(02)00250-7.

Etzelmüller, B., Czedirda, J., Magnin, F., Duvillard, P.A., Malet, E., Ravanel, L., Aspaas, A., Kristensen, L., Skrede, I., Majala, G.D., Jacobs, B., Leinauer, J., Hauck, C., Hilbich, C., Böhme, M., Hermanns, R., Eriksen, H.Ø., Krautblatter, M., Westermann, S., 2021. Permafrost in monitored unstable rock slopes in Norway – new insights from rock wall temperature monitoring, geophysical surveying and numerical modelling. Earth Surf. Dyn. Discuss. 1–55 https://doi.org/10.5194/esurf-2021-10.

Evans, S.G., Clague, J.J., 1994. Recent climate change and catastrophic geomorphic processes in mountain environments. Geomorphology 10, 107–128. https://doi.org/10.1016/0169-555X(94)90011-6.

Fabel, D., Ballantyne, C.K., Xu, S., 2012. Trimlines, blockfields, mountain-top erratics and the vertical dimensions of the last British-Irish Ice Sheet in NW Scotland. Quat. Sci. Rev. 55, 91–102. https://doi.org/10.1016/j.quascirev.2012.09.002.

Farbrot, H., Hipp, T.F., Etzelmüller, B., Isaksen, K., Ødegård, R.S., Schuler, T.V., Humlum, O., 2011. Air and Ground Temperature Variations Observed along Elevation and Continentality Gradients in Southern Norway [https://doi.org/10.1002/ppp.733]. Permafrost and Periglacial Processes 22 (4), 343–360. https://doi.org/10.1002/ppp.733.

Feuillet, T., Mercier, D., 2012. Post-little ice age patterned ground development on two pyrenean proglacial areas: from deglaciation to periglaciation. Geogr. Ann. A. 94, 363–376. https://doi.org/10.1111/j.1468-0459.2012.00459.x.

Fjellanger, J., Sørbel, L., Linge, H., Brook, E.J., Raisbeck, G.M., Yiou, F., 2006. Glacial survival of blockfields on the Varanger Peninsula, northern Norway. Geomorphology 82, 255–272. https://doi.org/10.1016/j.geomorph.2006.05.007.

French, H.M., 2018. The Periglacial Environment, 4th edition. Wiley, Chichester.

Gehrenkamper, J., Treter, U., 1983. Untersuchungen zur deglaziation und talentwicklung im Dørålen/Rondane (Norwegen). In: Schroeder-Lanz, H. (Ed.), Late- and Postglacial Oscillations of Glaciers: Glacial and Periglacial Forms. Balkema, Rotterdam, pp. 171–185.

Gisnås, K., Etzelmüller, B., Farbrot, H., Schuler, T.V., Westermann, S., 2013. Cryo GRID 1.0: permafrost distribution in Norway estimated by a Spatial numerical model. Permafr. Periglac. 24, 2–19. https://doi.org/10.1002/ppp.1765.

Gisnås, K., Etzelmüller, B., Lussana, C., Hjort, J., Sannel, B.K., Isaksen, K., Westermann, S., Kuhry, P., Christiansen, H.H., Frampton, A., Åkerman, J., 2017. Permafrost map for Norway. Sweden and Finland. Permafr. Periglac. 28, 359–378. https://doi.org/10.1002/ppp.1922.

Goehring, B.M., Brook, E.J., Linge, H., Raisbeck, G.M., Yiou, F., 2008. Beryllium-10 exposure ages of erratic boulders in Southern Norway and implications for the history of the Fennoscandian Ice Sheet. Quat. Sci. Rev. 27, 320–336. https://doi.org/10.1016/j.quascirev.2007.11.004.

Goodfellow, B.W., 2012. A granulometry and secondary mineral fingerprint of chemical weathering in periglacial landscapes and its application to blockfield origins. Quat. Sci. Rev. 57, 121–135. https://doi.org/10.1016/j.quascirev.2012.09.023.

Hilger, P., Hermanns, R.L., Czekirda, J., Myhra, K.S., Gosse, J.C., Etzelmüller, B., 2021. Permafrost as a first order control on long-term rock-slope deformation in (Sub-) Arctic Norway. Quat. Sci. Rev. 251, 106718 https://doi.org/10.1016/j.quascirev.2020.106718.

Hughes, A.L.C., Gyllencreutz, R., Lohne, Ø.S., Mangerud, J., Svendsen, J.I., 2016. The last Eurasian ice sheets – a chronological database and time-slice reconstruction, DATED-1. Boreas 45, 1–45. https://doi.org/10.1111/bor.12142.

Isaksen, K., Sollid, J.L., Holmlund, P., Harris, C., 2007. Recent warming of mountain permafrost in Svalbard and Scandinavia. J. Geophys. Res. 112, F92S04 https://doi.org/10.1029/2006JF000522.

Kerguillec, R., Sellier, D., 2015. Selection of geomorphosites in the Rondane National Park (central Norway): landforms and popularization. Géomorphologie 21, 131–144. https://doi.org/10.4000/geomorphologie.11012.

Kessler, M.A., Murray, A.B., Werner, T.B., Hallet, B., 2001. A model for sorted circles as self-organized patterns. J. Geophys. Res. Solid Earth 106, 13287–13306. https://doi.org/10.1029/2001JB000279.

King, L., 1984. In: Permafrost in Skandinavien: Untersuchungsergebnisse aus Lappland, Jotunheimen und Dovre/Rondane. Universität, Heidelberger Geographische Arbeiten, Heidelberg, p. 76.

Kłapyta, P., 2013. Application of Schmidt hammer relative age dating to late Pleistocene moraines and rock glaciers in the Western Tatra Mountains, Slovakia. Catena 111, 104–121. https://doi.org/10.1016/j.catena.2013.07.004.

Kleman, J., 2008. Geomorphology — where glaciers cut deep. Nat. Geosci. 1, 343–344. https://doi.org/10.1038/ngeo210.

Kvisvik, B.C., Paasche, Ø., Dahl, S.O., 2015. Holocene cirque glacier activity in Rondane, southern Norway. Geomorphology 246, 433–444. https://doi.org/10.1016/j.geomorph.2015.06.046.

Lilleøren, K.S., Etzelmüller, B., 2011. A regional inventory of rock glaciers and ice-cored moraines in Norway. Geogr. Ann. Ser. A 93, 175–191. https://doi.org/10.1111/j.1468-0459.2011.00430.x.

Lilleøren, K., Etzelmüller, B., Schuler, T.V., Gisnås, K., Humlum, O., 2012. The relative age of mountain permafrost – estimation of Holocene permafrost limits in Norway. Glob. Planet. Chang. 92–93, 209–223. https://doi.org/10.1016/j.gloplacha.2012.05.016.

Linge, H., Brook, E.J., Nesje, A., Raisbeck, G., Yiou, F., Clark, H., 2006. In situ 10Be exposure ages from southeastern Norway: implications for the geometry of the Weichselian scandinavian ice sheet. Quat. Sci. Rev. 25, 1097–1109. https://doi.org/10.1016/j.quascirev.2005.10.007.

Lohne, Ø.S., Mangerud, J., Birks, H.H., 2013. Precise 14C ages of the Vedde and Saksunarvatn ashes and the Younger Dryas boundaries from western Norway and their comparison with the Greenland Ice Core (GICC05) chronology. J. Quat. Sci. 28, 490–500. https://doi.org/10.1002/jqs.2640.

Luoto, M., Hjort, J., 2004. Generalized linear modeling in periglacial studies: terrain parameters and patterned ground. Permafr. Periglac. 15, 327–338. https://doi.org/10.1002/ppp.482.

Magnin, F., Etzelmüller, B., Westermann, S., Isaksen, K., Hilger, P., Hermanns, R.L., 2019. Permafrost distribution in steep rock slopes in Norway: measurements, statistical modelling and implications for geomorphological processes. Earth Surf. Dyn. 7 (4), 1019–1040. https://doi.org/10.5194/esurf-7-1019-2019.

Marr, P., Winkler, S., Löffler, J., 2018. Investigations on blockfields and related landforms at Blåhø (Southern Norway) using Schmidt-hammer exposure-age dating: palaeoclimatic and morphodynamic implications. Geogr. Ann. A. 100, 285–306. https://doi.org/10.1080/04353676.2018.1474350.

Marr, P., Winkler, S., Löffler, J., 2019a. Schmidt-hammer exposure age dating (SHD) performed on periglacial and related landforms in Opplendskedalen, Geirangerfjellet, Norway: implications for mid- and late-Holocene climate variability. The Holocene 29, 97–109. https://doi.org/10.1177/0959683618804634.

Marr, P., Winkler, S., Binnie, S.A., Löffler, J., 2019b. 10Be based exploration of the timing of deglaciation in two selected areas of southern Norway. E & G Quat. Sci. J. 68, 165–176. https://doi.org/10.5194/egqsj-68-165-2019.

Marr, P., Winkler, S., Löffler, J., 2019c. Aspects of late Weichselian deglaciation in South Norway: timing of deglaciation, ice sheet geometry, and climate variations inferred from surface exposure ages of late Pleistocene and Holocene landforms. Erdkunde 73, 277–301. https://doi.org/10.3112/erdkunde.2019.04.03.

Matthews, J.A., 1987. Regional variation in the composition of Neoglacial end moraines, Jotunheimen, Norway: an altitudinal gradient on clast roundness and its possible palaeoclimatic significance. Boreas 16, 173–188.

Matthews, J.A., Dresser, P.Q., 2008. Holocene glacier variation chronology of Smørstabbtindan massif, Jotunheimen, southern Norway, and the recognition of century- to millennial-scale European Neoglacial events. The Holocene 18, 181–201. https://doi.org/10.1177/0959683607085608.

Matthews, J.A., Owen, G., 2010. Schmidt hammer exposure-age dating: developing linear age-calibration curves using Holocene bedrock surfaces from the Jotunheimen-Jostedalsbreen regions of southern Norway. Boreas 39, 105–115. https://doi.org/10.1111/j.1502-3885.2009.00107.x.

Matthews, J.A., Wilson, P., 2015. Improved Schmidt-hammer exposure ages for active and relict pronival ramparts in southern Norway, and their palaeoenvironmental implications. Geomorphology 246, 7–21. https://doi.org/10.1016/j.geomorph.2015.06.002.

Matthews, J.A., Winkler, S., 2011. Schmidt-hammer exposure-age dating (SHD): application to early Holocene moraines and a reappraisal of the reliability of terrestrial cosmogenic-nuclide dating (TCND) at Austanbotnbreen, Jotunheimen, Norway. Boreas 40, 256–270. https://doi.org/10.1111/j.1502-3885.2010.00178.x.

Matthews, J.A., Dahl, S.-O., Dresser, P.Q., Berrisford, M.S., Lie, Ø., Nesje, A., Owen, G., 2009. Radiocarbon chronology of Holocene colluvial (debris-flow) activity at Sletthamn, Jotunheimen, southern Norway: a window on the changing frequency of extreme climatic events and their landscape impact. The Holocene 19, 1107–1129. https://doi.org/10.1177/0959683609344674.

Matthews, J.A., Shakesby, R.A., Owen, G., Vater, A.E., 2011. Pronival rampart formation in relation to snow-avalanche activity and Schmidt-hammer exposure-age dating (SHD): three case studies from southern Norway. Geomorphology 130, 280–288. https://doi.org/10.1016/j.geomorph.2011.04.010.

Matthews, J.A., Nesje, A., Linge, H., 2013. Relict talus-foot rock glaciers at Øyberget, Upper Ottadalen, Southern Norway: Schmidt hammer exposure ages and palaeoenvironmental implications. Permafr. Periglac. 24, 336–346. https://doi.org/10.1002/ppp.1794.

Matthews, J.A., Winkler, S., Wilson, P., 2014. Age and origin of ice-cored moraines in Jotunheimen and Breheimen, Southern Norway: insights from Schmidt-hammer exposure-age dating. Geogr. Ann. A 96, 531–548. https://doi.org/10.1111/geoa.12046.

Matthews, J.A., McEwen, L., Owen, G., 2015. Schmidt-hammer exposure-age dating (SHD) of snow-avalanche impact ramparts in southern Norway: approaches, results and implications for landform age, dynamics and development. Earth Surf. Process. Landf. 40, 1705–1718. https://doi.org/10.1002/esp.3746.

Matthews, J.A., Owen, G., Winkler, S., Vater, A.E., Wilson, P., Mourne, R.W., Hill, J.L., 2016. A rock-surface microweathering index from Schmidt hammer R-values and its preliminary application to some common rock types in southern Norway. Catena 143, 35–44. https://doi.org/10.1016/j.catena.2016.03.018.

Matthews, J.A., Winkler, S., Wilson, P., Tomkins, M., Dortch, J., Mourne, R., Hill, J., Owen, G., Tomkins, J., Vater, A., 2018. Small rock-slope failures conditions by Holocene permafrost degradation: a new approach and conceptual model based on Schmidt-hammer exposure-age dating in Jotunheimen, southern Norway. Boreas 47, 1144–1169. https://doi.org/10.1111/bor.12336.

Matthews, J.A., Haselberger, S., Hill, J.L., Owen, G., Winkler, S., Hiemstra, J.F., Hallang, H., 2020a. Snow-avalanche boulder fans in Jotunheimen, southern Norway: Schmidt-hammer exposure-age dating, geomorphometrics, dynamics and evolution. Geogr. Ann. A. 102, 118–140. https://doi.org/10.1080/04353676.2020.1762365.

Matthews, J.A., McEwen, L.J., Owen, G., Los, S., 2020b. Holocene alluvial fan evolution, Schmidt-hammer exposure-age dating and paraglacial debris floods in the SE Jostedalsbreen region, southern Norway. Boreas 49, 886–904. https://doi.org/10.1111/bor.12456.

McColl, S.T., 2012. Paraglacial rock-slope stability. Geomorphology 153–154, 1–16. https://doi.org/10.1016/j.geomorph.2012.02.015.

McEwen, L.J., Matthews, J.A., Owen, G., 2020. Development of a Holocene glacier-fed alluvial fan based on calibrated- and relative age dating techniques: the Illåe fan, Jotunheimen, Norway. Geomorphology 363, 107200. https://doi.org/10.1016/j.geomorph.2020.107200.

Nesje, A., 2009. Latest Pleistocene and Holocene alpine glacier fluctuations in Scandinavia. Quat. Sci. Rev. 28, 2119–2136. https://doi.org/10.1016/j.quascirev.2008.12.016.

Nesje, A., Dahl, S.O., 2001. The Greenland 8200 cal. Yr BP event detected in loss-on-ignition profiles in Norwegian lacustrine sediment sequences. J. Quat. Sci. 16, 155–166. https://doi.org/10.1002/jqs.567.

Nesje, A., Kvamme, M., 1991. Holocene glacier and climate variations in western Norway: evidence for early Holocene glacier demise and multiple Neoglacial events. Geology 19, 610–612. https://doi.org/10.1130/0091-7613(1991)019<0610:HGACVI>2.3.CO;2.

Nesje, A., Kvamme, M., Rye, N., Løvlie, R., 1991. Holocene glacial and climatic history of the Jostedalsbreen region, western Norway: evidence from lake sediments and terrestrial deposits. Quat. Sci. Rev. 10, 97–114.

Nesje, A., Matthews, J.A., Dahl, S.O., Berrisford, M.S., Andersson, C., 2001. Holocene glacier fluctuations of Flatebreen and winter precipitation changes in the Jostedalsbreen region, western Norway, based on glaciolacustrine records. The Holocene 11, 267–280. https://doi.org/10.1191/095968301669980885.

Nesje, A., Matthews, J.A., Linge, H., Bredal, M., Wilson, P., Winkler, S., 2021. New evidence of active talus-foot rock glaciers at Øyberget, southern Norway, and their development during the Holocene. The Holocene 31, 1786–1796, 10.1177%2F09596836211033226.

Nicholson, D.T., 2008. Rock control in microweathering of bedrock surfaces in a periglacial environment. Geomorphology 101, 655–665. https://doi.org/10.1016/j.geomorph.2008.03.009.

Niedzielski, T., Migon, P., Placek, A., 2009. A minimum sample size required from Schmidt hammer measurements. Earth Surf. Process. Landf. 34 (13), 1713–1725.

Ødegård, R.S., Sollid, J.L., Liestøl, O., 1988. Periglacial forms related to terrain parameters in Jotunheimen, southern Norway. In: Senneset, K. (Ed.), 5th International Conference on Permafrost Proceedings. 3. Tapir, Trondheim, pp. 59–61.

Oftedahl, C., 1950. Petrology and geology of the Rondane area. Nor. Geol. Tidsskr. 28, 199–225.

Paasche, Ø., Støren, E.N., 2014. How does climate impact floods? Closing the knowledge gap. Eos 95, 253–254. https://doi.org/10.1002/2014EO280001.

Patton, H., Hubbard, A., Andreassen, K., Winsborrow, M., Stroeven, A.P., 2016. The buildup, configuration, and dynamical sensitivity of the Eurasian ice-sheet complex to late Weichselian climatic and oceanic forcing. Quat. Sci. Rev. 153, 97–121. https://doi.org/10.1016/j.quascirev.2016.10.009.

Paus, A., Haflidason, H., Routh, J., Naafs, B.D.A., Thoen, M.W., 2019. Environmental responses to the 9.7 and 8.2 cold events at two ecotonal sites in the Dovre mountains, mid-Norway. Quat. Sci. Rev. 205, 45–61. https://doi.org/10.1016/j.quascirev.2018.12.009.

Powers, M.S., 1953. A new roundness scale for sedimentary particles. J. Sediment. Petrol. 23, 117–119. https://doi.org/10.1306/D4269567-2B26-11D7-8648000102C1865D.

Proceq, 2014. Operating Instructions RockSchmidt & Rocklink. Proceq SA, Schwerzenbach.
Ramberg, I., Bryhni, I., Nøttvedt, A., Rangnes, K., 2008. The Making of a Land – Geology of Norway. Trondheim (NGF).
Rea, B.R., Whalley, W., Rainey, M.M., Gordon, J.E., 1996. Blockfields, old or new? Evidence and implications from some plateaus in northern Norway. Geomorphology 15, 109–121. https://doi.org/10.1016/0169-555X(95)00118-O.
Rode, M., Kellerer-Pirklbauer, A., 2011. Schmidt-hammer exposure-age dating (SHD) of rock glaciers in the Schöderkogel-Eisenhut area, Schladminger Tauern Range, Austria. The Holocene 22, 761–771. https://doi.org/10.1177/0959683611430410.
Sellier, D., Kerguillec, R., 2021. Characterization of scree slopes in the Rondane Mountains (South-Central Norway). In: Beylich, A.A. (Ed.), Landscapes and Landforms of Norway. Springer, Cham, pp. 203–223.
Shakesby, R.A., Dawson, A.G., Matthews, J.A., 1987. Rock glaciers, protalus ramparts and related phenomena, Rondane, Norway — a continuum of large-scale talus-derived landforms. Boreas 16, 305–317.
Shakesby, R.A., Matthews, J.A., Owen, G., 2006. The Schmidt hammer as a relative-age dating tool and its potential for calibrated-age dating in Holocene glaciated environments. Quat. Sci. Rev. 25, 2846–2867. https://doi.org/10.1016/j.quascirev.2006.07.011.
Shakesby, R.A., Matthews, J.A., Karlén, W., Los, S.O., 2011. The Schmidt hammer as a Holocene calibrated-age dating technique: testing the form of the R-value-age relationship and defining the predicted-age errors. The Holocene 21, 615–628. https://doi.org/10.1177/0959683610391322.
Shakesby, R.A., Matthews, J.A., Winkler, S., Fabel, D., Dresesr, P.Q., 2020. Early-Holocene moraine chronology, Sognefjell area, southern Norway: evidence for multiple glacial and climatic fluctuations within the Erdalen Event (~10.2–9.7 ka). Nor. Geol. Tidsskr. 100, 202014 https://doi.org/10.17850/njg100-3-2.
Sigmond, E.M.O., Gustavson, M., Roberts, D., 1986. Berggrunnskart over Norge. 1:100 000. Nasjonal atlas for Norge. Norges Geologiske Undersøkelse, Trondheim.
Sollid, J., Sørbel, L., 1994. Distribution of glacial landforms in southern Norway in relation to the thermal regime of the last continental ice sheet. Geogr. Ann. A 76, 25–35. https://doi.org/10.1080/04353676.1994.11880403.
Støren, E.N., Paasche, Ø., 2014. Scandinavian floods: from past observations to future trends. Glob. Planet. Chang. 113, 34–43. https://doi.org/10.1016/j.gloplacha.2013.12.002.
Stroeven, A.P., Hättestrand, C., Kleman, J., Heyman, J., Fabel, D., Fredin, O., Goodfellow, B.W., Harbor, J.M., Jansen, J.D., Olsen, L., Caffee, M.W., Fink, D., Lundqvist, J., Rosqvist, G.C., Strömberg, B., Jansson, K.N., 2016. Deglaciation of Fennoscandia. Quat. Sci. Rev. 147, 91–121. https://doi.org/10.1016/j.quascirev.2015.09.016.
Strøm, K., 1945. Geomorphology of the Rondane area. Nor. Geol. Tidsskr. 25, 360–378.
Tomkins, M.D., Dortch, J.M., Hughes, P.D., 2016. Schmidt hammer exposure dating (SHED): establishment and implications for the retreat of the last British Ice Sheet. Quat. Geochronol. 33, 46–60. https://doi.org/10.1016/j.quageo.2016.02.002.
Tomkins, M.D., Dortch, J.M., Hughes, P.D., Huck, J.J., Stimson, A.G., Delmas, M., Calvet, M., Pallàs, R., 2018. Schmidt hammer exposure dating (SHED): rapid age assessment of glacial landforms in the Pyrenees. Quat. Res. 90, 26–37. https://doi.org/10.1017/qua.2018.12.
Tveten, E., Lutro, O., Thorsnes, T., 1998. Geologisk kart over Norge, 1:250,000. Norges Geologiske Undersøkelse, Trondheim.
Vandenberghe, J., 1988. Cryoturbations. In: Clark, M.J. (Ed.), Advances in Periglacial Geomorphology. Wiley, Chichester, pp. 179–198.
Vasskog, K., Nesje, A., Støren, E.N., Waldmann, N., Chapron, E., Ariztegui, D., 2011. A Holocene record of snow-avalanche and flood activity reconstructed from a lacustrine sedimentary sequence in Oldevatnet, western Norway. The Holocene 21, 1–18. https://doi.org/10.1177/0959683610391316.
Washburn, A.L., 1956. Classification of patterned ground and review of suggested origins. Geol. Soc. Am. Bull. 67, 823–865. https://doi.org/10.1130/0016-7606(1956)67[823, COPGAR]2.0.CO;2.
Washburn, A.L., 1979. Geocryology, 2nd edition. Arnold, London.
Whittecar, G.R., Ryter, D.W., 1992. Boulder streams, debris fans and Pleistocene climate change in the blue ridge mountains of Central Virginia. J. Geol. 100, 487–494.
Williams, G., 1983. Paleohydrological methods and some examples from swedish fluvial environments: I. Cobble and boulder deposits. Geogr. Ann. A. 65A, 224–243.
Wilson, P., 2007. Block/rock streams. In: Elias, S. (Ed.), Encyclopedia of Quaternary Science. Elsevier, Oxford, pp. 2218–2225.
Wilson, P., Matthews, J.A., 2016. Age assessment and implications of late Quaternary periglacial and paraglacial landforms on Muckish Mountain, Northwest Ireland, based on Schmidt-hammer exposure-age dating (SHD). Geomorphology 270, 134–144. https://doi.org/10.1016/j.geomorph.2016.07.002.
Wilson, P., Bentley, M.J., Schnabel, C., Clark, R., Xu, S., 2008. Stone run (block stream) formation in the Falkland Islands over several cold stages, deduced from cosmogenic isotope (10Be and 26Al) surface exposure dating. J. Quat. Sci. 23, 461–473. https://doi.org/10.1002/jqs.1156.
Wilson, P., Matthews, J.A., Mourne, R.W., 2017. Relict Blockstreams at Insteheia, Valldalen-Tafjorden, Southern Norway: their nature and Schmidt Hammer exposure age. Permafr. Periglac. 28, 286–297. https://doi.org/10.1002/ppp.1915.
Wilson, P., Matthews, J.A., Mourne, R.W., Linge, H., Olsen, J., 2020. Interpretation, age and significance of a relict paraglacial and periglacial boulder-dominated landform assemblage in Alnesdalen, Romsdalsalpane, southern Norway. Geomorphology 369, 107362. https://doi.org/10.1016/j.geomorph.2020.107362.
Winkler, S., 2014. Investigation of late-Holocene moraines in the western Southern Alps, New Zealand, applying Schmidt-hammer exposure-age dating (SHD). The Holocene 24, 48–66. https://doi.org/10.1177/0959683613512169.
Winkler, S., Lambiel, C., 2018. Age constraints of rock glaciers in the Southern Alps/New Zealand – exploring their palaeoclimatic potential. The Holocene 28, 778–790. https://doi.org/10.1177/0959683618756802.
Winkler, S., Matthews, J.A., 2014. Comparison of electronic and mechanical Schmidt hammers in the context of exposure-age dating: are Q- and R-values interconvertible? Earth Surf. Process. Landf. 39, 1128–1136. https://doi.org/10.1002/esp.3584.
Winkler, S., Matthews, J.A., Mourne, R.W., Wilson, P., 2016. Schmidt-hammer exposure ages from periglacial patterned ground (sorted circles) in Jotunheimen, Norway, and their interpretative problems. Geogr. Ann. A 98, 265–285. https://doi.org/10.1111/geoa.12134.
Winkler, S., Matthews, J.A., Haselberger, S., Hill, J.L., Mourne, R.W., Owen, G., Wilson, P., 2020. Schmidt-hammer exposure-age dating (SHD) of sorted stripes on Juvflye, Jotunheimen (central South Norway): morphodynamic and palaeoclimatic implications. Geomorphology 353, 107014. https://doi.org/10.1016/j.geomorph.2019.107014.
Winkler, S., Donner, A., Tintrup gen. Suntrup, A., 2021. Periglacial landforms in Jotunheimen, Central Southern Norway, and their altitudinal distribution. In: Beylich, A.A. (Ed.), Landscapes and Landforms of Norway. Springer, Cham, pp. 169–202.
www.ngu.no – Geological Survey of Norway/www.ngu.no (last accessed 29.01.2022) 2022.
www.norgeibilder.no – open portal of Kartverket/www.kartverket.no (last accessed 20.12.2020) 2020.
www.senorge.no – open portal in collaboration between Norges Vassdrags- og Energi direktoratet/www.nve.no, Meteorologisk institutt/www.met.no, and Kartverket/www.kartverket.no (last accessed 20.12.2020) 2020.
www.met.no – open portal of Meteorologisk insitutt/www.met.no (last accessed 21.01.2022).